



HAL
open science

Idealized multiple-timescale model of cortical spreading depolarization initiation and pre-epileptic hyperexcitability caused by NaV1.1/SCN1A mutations

Louisiane Lemaire, Mathieu Desroches, Martin Krupa, Massimo Mantegazza

► **To cite this version:**

Louisiane Lemaire, Mathieu Desroches, Martin Krupa, Massimo Mantegazza. Idealized multiple-timescale model of cortical spreading depolarization initiation and pre-epileptic hyperexcitability caused by NaV1.1/SCN1A mutations. *Journal of Mathematical Biology*, 2023, 86 (6), pp.92. 10.1007/s00285-023-01917-5 . hal-04108905

HAL Id: hal-04108905

<https://hal.science/hal-04108905>

Submitted on 29 May 2023

HAL is a multi-disciplinary open access archive for the deposit and dissemination of scientific research documents, whether they are published or not. The documents may come from teaching and research institutions in France or abroad, or from public or private research centers.

L'archive ouverte pluridisciplinaire **HAL**, est destinée au dépôt et à la diffusion de documents scientifiques de niveau recherche, publiés ou non, émanant des établissements d'enseignement et de recherche français ou étrangers, des laboratoires publics ou privés.

Idealized multiple-timescale model of cortical spreading depolarization initiation and pre-epileptic hyperexcitability caused by $\text{Na}_V1.1/SCN1A$ mutations

Louisiane Lemaire^{*1,2,3}, Mathieu Desroches¹, Martin Krupa^{1,4}, and Massimo Mantegazza^{5,6,7}

¹Inria at Université Côte d’Azur, MathNeuro Project-Team, Valbonne-Sophia Antipolis, France

²Humboldt-University of Berlin, Institute for Theoretical Biology, Berlin, Germany

³Bernstein Center for Computational Neuroscience, Berlin, Germany

⁴Université Côte d’Azur, Laboratoire Jean-Alexandre Dieudonné, Nice, France

⁵Université Côte d’Azur, Institute of Molecular and Cellular Pharmacology (IPMC), Valbonne-Sophia Antipolis, France

⁶CNRS UMR7275, Institute of Molecular and Cellular Pharmacology (IPMC), Valbonne-Sophia Antipolis, France

⁷INSERM, Valbonne-Sophia Antipolis, France

Abstract

$\text{Na}_V1.1$ (*SCN1A*) is a voltage-gated sodium channel mainly expressed in GABAergic neurons. Loss of function mutations of $\text{Na}_V1.1$ lead to epileptic disorders, while gain of function mutations cause a migraine in which cortical spreading depolarizations (CSDs) are involved. It is still debated how these opposite effects initiate two different manifestations of neuronal hyperactivity: epileptic seizures and CSD.

To investigate this question, we previously built a conductance-based model of two neurons (GABAergic and pyramidal), with dynamic ion concentrations (Lemaire et al. in PLOS Comput. Biol. 17(7):e1009239, 2021). When implementing either $\text{Na}_V1.1$ migraine or epileptogenic mutations, ion concentration modifications acted as slow processes driving the system to the corresponding pathological firing regime. However, the large dimensionality of the model complicated the exploitation of its implicit multi-timescale structure.

Here, we substantially simplify our biophysical model to a minimal version more suitable for bifurcation analysis. The explicit timescale separation allows us to apply slow-fast theory, where slow variables are treated as parameters in the fast singular limit. In this setting, we reproduce both pathological transitions as dynamic bifurcations in the full system. In the epilepsy condition, we shift the spike-terminating bifurcation to lower inputs for the GABAergic neuron, to model an increased susceptibility to depolarization block. The resulting failure of synaptic inhibition triggers hyperactivity of the pyramidal neuron. In the migraine scenario, spiking-induced release of potassium leads to the abrupt increase of the extracellular potassium concentration. This causes a dynamic spike-terminating bifurcation of both neurons, which we interpret as CSD initiation.

1 Introduction

$\text{Na}_V1.1$ is a voltage-gated sodium channel, coded by the gene *SCN1A*, which is mainly expressed in GABAergic neurons. It is a major target of human mutations implicated in pathologies of neuronal excitability [32, 34]. In the case of so-called loss of function mutations, the mutated $\text{Na}_V1.1$ channels are partially or fully inactive, resulting in reduced sodium current. Such mutations have been found in patients with epileptic disorders. This is for example the case of Dravet syndrome [10, 46], a severe form of epilepsy, characterized by drug-resistant seizures and developmental delay. On the other hand, gain of function mutations of $\text{Na}_V1.1$ —i.e. mutations enhancing channel activity—have been linked to familial hemiplegic migraine type 3 (FHM3) [16, 7, 15, 33]. More precisely, those mutations impair the mechanism of inactivation of the channels, which induces an increased persistent sodium current. FHM3 is a severe subtype of migraine with aura, for which a proposed pathological mechanism is cortical spreading depolarization (CSD), a wave of transient intense neuronal firing followed by a sustained depolarization block, which slowly propagates in the cortex [37, 33]. A recent report provides clinical evidence linking this wave and the migraine aura [31], and it has been suggested that CSD also causes the headache, through the stimulation of meningeal trigeminal nociceptors [19]. However, it is still debated how $\text{Na}_V1.1$ gain of function contributes to CSD initiation and how loss of function of the same channel leads to seizure onset. To investigate those pathological mechanisms, we previously developed a detailed conductance-based model of two neurons, a GABAergic and a pyramidal neuron, with dynamic ion concentrations [29]. In the present study we continue this modeling work, but in a simpler framework which is more amenable to theoretical analysis.

*louisiane.lemaire@hu-berlin.de

$\text{Na}_V1.1$ gain of function facilitates CSD induction, both in our detailed computational model [29] and in experimental systems (FHM3 mouse models [25, 2] and acute pharmacological activation of the channel [9]). We have shown that neither GABAergic nor glutamatergic synaptic transmission is required for the initiation of this wave [9]. Instead, a key factor for CSD initiation in the case of FHM3 seems to be a progressive build up of extracellular potassium, generated by the spiking of GABAergic neurons, which engages the network in a positive loop of hyperexcitability and extracellular potassium build up, leading to depolarization block of the entire network [29, 9, 2].

The prevailing hypothesis concerning the pathological mechanism of $\text{Na}_V1.1$ epileptogenic mutations is the hypoexcitability of GABAergic neurons [32], which reduces synaptic inhibition, promoting hyperexcitability of neuronal networks. Experiments in mouse models of Dravet syndrome suggest that this initial direct effect of the mutations leads to further network alterations, which may contribute to the phenotype at later stages of the disease [26, 1, 40]. Here, as in our previous paper [29], we focus on the early period of pre-epileptic hyperexcitability, during which spontaneous seizures are typically not observed [30, 36]. In our detailed model [29], $\text{Na}_V1.1$ epileptogenic mutations made the GABAergic neuron more susceptible to depolarization block: the external input necessary to trigger this transition was smaller than in the control condition. Importantly, depolarization block of the GABAergic neuron was associated with hyperactivity of the pyramidal neuron. This, together with other experimental [5, 47, 6] and computational studies [27], supports the hypothesis that depolarization block of GABAergic neurons and the resulting failure of inhibitory restraint is a mechanism giving rise to network hyperexcitability.

In this paper, we are interested in dynamic bifurcation scenarios which can be associated with the onset of CSD or epileptiform activity caused by $\text{Na}_V1.1$ mutations in a multiple-timescale idealized model. Slow-fast dissection [39, 38] is indeed a powerful tool to study the spectrum of activity regimes in the neuronal context. We initiated this approach in [29] (see Fig. 11), however the size of the model made it prohibitive to perform a thorough analysis. For this reason, we build here a 6-dimensional minimal version of the detailed biophysical model. To keep it as simple as possible, we mainly use polynomial terms, except for the modeling of the aspects which are suspected to play an essential role in the pathological mechanisms of $\text{Na}_V1.1$ mutations: spiking-induced release of potassium in the case of migraine and synaptic inhibition in the case of epilepsy.

We design the idealized system in such a way to have three explicit timescales. Neuronal dynamics is the fastest, both neurons being modeled by a two-dimensional oscillator. The extracellular potassium concentration is then an obvious choice of slow variable to drive the system to pathological regimes. Several computational studies have shown that neurons depolarization block can be modeled as a slow passage through a Hopf bifurcation, driven by a build-up of potassium in the extracellular space [3, 21, 45, 43]. Unlike those, in which the pathological behavior is often obtained by increasing the potassium concentration in a distant reservoir, we directly implement the effect of the mutations on the firing properties of the GABAergic neuron, and examine the response of the pyramidal neuron. Furthermore, based on Hübel et al., we introduce a third timescale which is even slower than the potassium [24], an approach also used in [43]. This choice is motivated by the characteristic potassium dynamics at the site of CSD initiation shown in Fig. 1. The initial progressive accumulation is followed by an abrupt increase, which hints at an additional timescale underlying potassium dynamics.

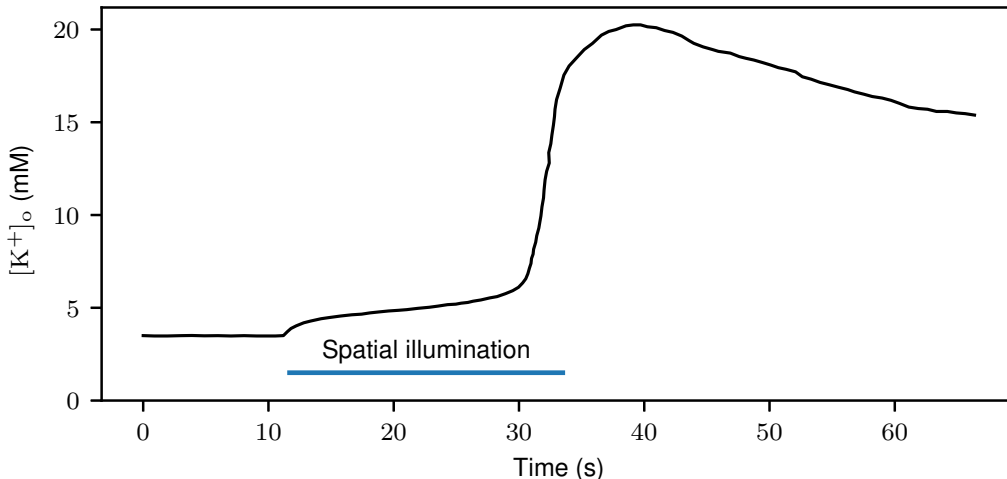


Figure 1: Extracellular potassium dynamics at the site of CSD initiation. We reproduce here the potassium trace shown in Fig. 8 of [9], which was recorded at the site of CSD initiation. Spatial optogenetic illumination was used to induce hyperactivity of GABAergic neurons in a predetermined area of the cortex, in order to specifically control the area of CSD initiation, allowing recordings at the initiation site.

We first perform numerical continuation with the software package AUTO [17], to unravel the complicated bifurcation structure of the fast layer problem. We then study the slow dynamics of the potassium concentration with tools from dynamical systems theory such as phase-plane analysis and invariant manifolds. Finally, we gather information obtained from the slow and fast components to interpret the dynamics of the full system, namely transitions from physiological

firing to CSD and epileptiform hyperactivity.

2 Model

We consider a pair of neurons: a pyramidal neuron (x_e, y_e) and a GABAergic interneuron (x_i, y_i) . Each neuron is modeled using a modified Hindmarsh–Rose system (see Section 2.2). They can be stimulated by an external current I_{ext} . We implemented an inhibitory synapse from the GABAergic neuron to the pyramidal one, with the current I_{GABA} (see Section 2.3). We also modeled the dynamics of the extracellular potassium, using a two-dimensional system $([\text{K}]_o^+, w)$ (see Section 2.4). The firing of the neurons releases potassium in the extracellular space, which we account for with the terms $pg(x_i)$ and $g(x_e)$ (see Sections 2.5 and 2.6). Conversely, we take into account the depolarizing effect of extracellular potassium on the neurons. The overall system has three main timescales, see Section 2.1.

The dynamics of the full system is given in (1). Fig. 2 shows a schematic representation of the system. The state variables are listed in Table 1 and the model parameters in Table 2.

$$\frac{dx_e}{dt} = c_e \left(x_e - \frac{x_e^3}{3} - y_e + [\text{K}]_o^+ + I_{\text{ext}} - I_{\text{GABA}}(x_e, x_i) \right) \quad (1a)$$

$$\frac{dy_e}{dt} = \frac{x_e^2 + dx_e - by_e + a}{c_e} \quad (1b)$$

$$\frac{dx_i}{dt} = c_i \left(x_i - \frac{x_i^3}{3} - y_i + [\text{K}]_o^+ + I_{\text{ext}} \right) \quad (1c)$$

$$\frac{dy_i}{dt} = \frac{x_i^2 + dx_i - by_i + a}{c_i} \quad (1d)$$

$$\frac{d[\text{K}]_o^+}{dt} = \varepsilon (w - f([\text{K}]_o^+) + pg(x_i) + g(x_e)) \quad (1e)$$

$$\frac{dw}{dt} = \varepsilon \delta (-[\text{K}]_o^+ - \alpha + \beta w) \quad (1f)$$

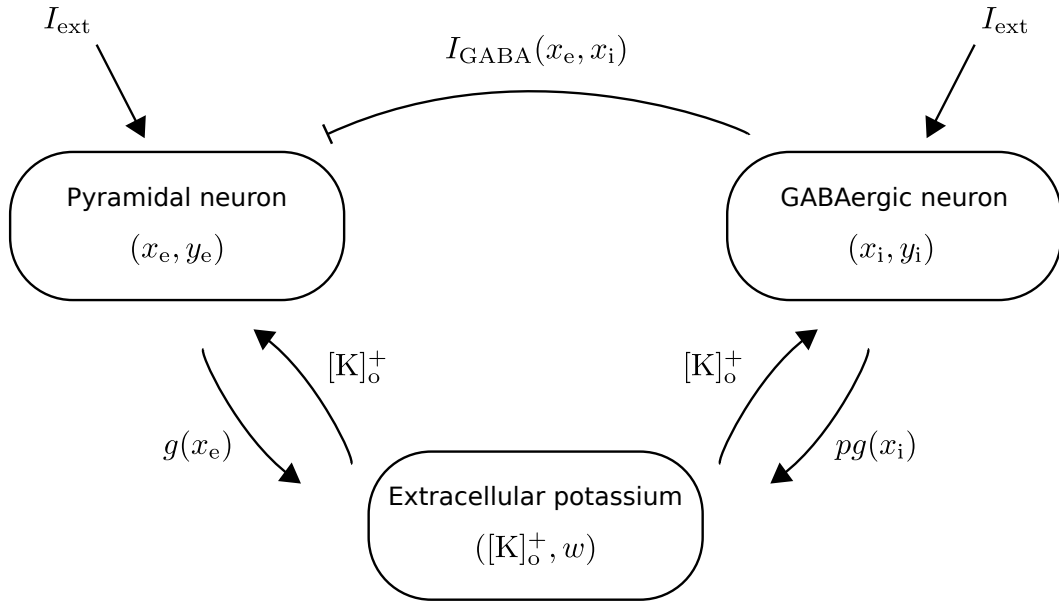


Figure 2: Schematic representation of the model.

2.1 Slow-fast structure

By construction, there are three main timescales in the six-dimensional model defined by System (1):

- The neuron variables (x_e, y_e, x_i, y_i) are faster than the potassium ones $([\text{K}]_o^+, w)$, through the presence of the small parameter $0 < \varepsilon \ll 1$, which we set to be of order 10^{-3} in simulations (Table 2). We call the four-dimensional subsystem (x_e, y_e, x_i, y_i) the fast block and the two-dimensional subsystem $([\text{K}]_o^+, w)$ the slow block or potassium block.
- Inside this slow block, there are also two separated timescales, $[\text{K}]_o^+$ being faster than w due to the small parameter $0 < \delta \ll 1$. See Section 4 for a detailed study of the potassium block.

Table 1: *State variables*

Symbol	Description	Timescale
x_e	Membrane potential of the pyramidal neuron	Fast
y_e	Gating variable for the pyramidal neuron	Fast
x_i	Membrane potential of the GABAergic neuron	Fast
y_i	Gating variable for the GABAergic neuron	Fast
$[K]_o^+$	Extracellular potassium concentration	Slow
w	Additional variable for the dynamics of $[K]_o^+$	Superslow

Table 2: *Model parameters*

	Symbol	Description	Value
	I_{ext}	External input	0.35
Slow-fast structure			
	ε	$([K]_o^+, w)$ vs. neurons	0.002
	δ	w vs. $[K]_o^+$	0.005
Neuronal dynamics			
	a		0.56 [14]
	b		1.2
	c_e	c for the pyramidal neuron	3 [14]
	c_i	c for the GABAergic neuron	Wild-type: 3 [14] Epilepsy: 1.2
	d		1.8
Inhibitory synapse			
	g_{GABA}	Maximal conductance	15
	E_{GABA}	Reversal potential	-2.5
	k_{GABA}	Sigmoids slope parameter	20
	$\theta_{\text{GABA},1}$	Increasing sigmoid midpoint	-1
	$\theta_{\text{GABA},2}$	Decreasing sigmoid midpoint	0.1
$[K]_o^+$ dynamics			
	z_l	$[K]_o^+$ -nullcline local maximum ¹	0.5
	z_r	$[K]_o^+$ -nullcline local minimum ¹	1.5
	β	Controls w -nullcline slope ¹	-13
	α	Controls w -nullcline intercept ¹	-2.6
K^+ release			
	g_K	Maximal neuronal contribution	0.015
	k_K	Sigmoid slope parameter	10
	θ_K	Sigmoid midpoint	0.6
	p	K^+ release scaling factor	Wild-type: 1 Migraine: 4

System (1) is therefore a slow-fast system with four fast, one slow and one superslow variable.

Note that w does not enter the equations of the fast block. By definition, letting $\varepsilon \rightarrow 0$ in System (1) yields the *fast layer problem* [13]. It corresponds to freezing the dynamics of $[K]_o^+$ and considering it as a parameter of the fast block (x_e, y_e, x_i, y_i) . In Section 3, we will study the bifurcation structure of the fast layer problem to better understand the dynamic transitions in the full system (1).

Inside each neuron model, the membrane potential $x_{e,i}$ is faster than the variable $y_{e,i}$ which models ion channels dynamics. This timescale separation, which we do not analyze as such in this work, is organized by the parameters $c_{e,i}$. However we exploit it to obtain the transition to epileptiform hyperactivity (see Section 2.6.2).

2.2 Neuronal dynamics

We model each neuron with a two-dimensional system inspired from Hindmarsh and Rose:

$$\begin{aligned}\frac{dx}{dt} &= c \left(x - \frac{x^3}{3} - y + I \right) \\ \frac{dy}{dt} &= \frac{x^2 + dx - by + a}{c}\end{aligned}\tag{2}$$

We took most parameter values from [14], except for b which we increased to shift the fold bifurcation of limit cycles responsible for the transition to depolarization block to larger values of I (Table 2). Compared to the original model [23], System (2) has been modified [42] so that spike generation is mediated by a SNIC instead of a saddle homoclinic bifurcation (Fig. 3). It exhibits thus class 1 excitability.

This is consistent with the experimental input-output relationships in Fig. 2 of [9]. They were recorded in neocortical pyramidal and fast-spiking GABAergic neurons of mice, before or during the application of the toxin Hm1a which mimics the effect of $\text{Na}_V1.1$ migraine mutations. It is also consistent with Fig. 4 and Supplementary Fig. 4 of [2], for cortical fast-spiking and regular spiking GABAergic neurons of wild-type or heterozygous $\text{Scn1a}^{+/- \text{L1649Q}}$ knock-in mice.

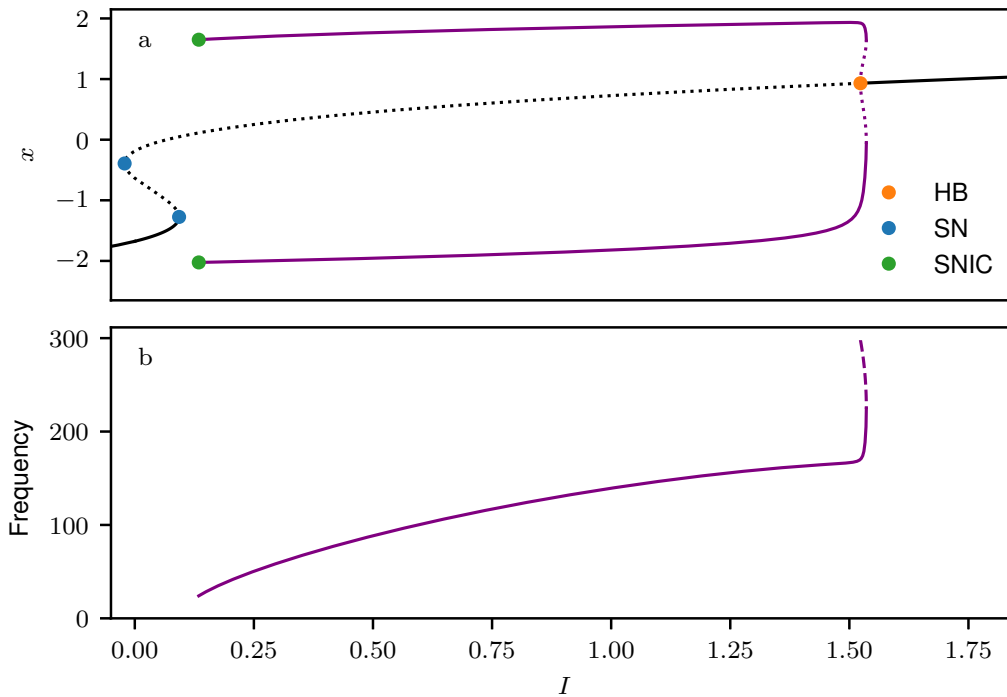


Figure 3: Dynamics of a single neuron. (a) Bifurcation diagram x vs. I of System (2). The black curves show families of stable (solid line) or unstable (dashed line) steady states. The purple lines show families of stable or unstable limit cycles. HB: Hopf bifurcation, here subcritical. SN: Saddle-node bifurcation of steady states. SNIC: saddle-node on invariant circle bifurcation. (b) Frequency of the limit cycles.

2.3 Inhibitory synapse

Although this model is very simplified with respect to the one developed and studied in [29], we did not remove the GABAergic synapse from the GABAergic neuron to the pyramidal one. This inhibitory connection is especially important in the case of the epileptogenic mutations of $\text{Na}_V1.1$ (see Section 5.2).

To keep the model as simple as possible, we decided not to use any additional synaptic variable or resetting rule. Instead, we scale the maximal conductance g_{GABA} of the inhibitory synaptic current I_{GABA} by a function s of the voltage:

$$I_{\text{GABA}} = g_{\text{GABA}} s(x_i) (x_e - E_{\text{GABA}}).$$

The function s is inspired from [8]. However, to prevent inhibition during depolarization block of the GABAergic neuron, we multiply the increasing sigmoid by a decreasing sigmoid of larger midpoint:

$$s(x_i) = \frac{1}{1 + e^{-k_{\text{GABA}}(x_i - \theta_{\text{GABA},1})}} \frac{1}{1 + e^{-k_{\text{GABA}}(-x_i + \theta_{\text{GABA},2})}}.$$

2.4 $[\text{K}]_o^+$ dynamics

To model the dynamics of the extracellular potassium, we use a two-dimensional slow-fast block, w being slower than $[\text{K}]_o^+$:

$$\begin{aligned}\frac{d[\text{K}]_o^+}{dt} &= w - f([\text{K}]_o^+) + g_{\text{tot}} \\ \frac{dw}{dt} &= \delta(-[\text{K}]_o^+ - \alpha + \beta w)\end{aligned}\tag{3}$$

where

$$f([\text{K}]_o^+) = \frac{([\text{K}]_o^+)^3}{3} - \frac{1}{2}(z_l + z_r)([\text{K}]_o^+)^2 + z_l z_r [\text{K}]_o^+.$$

This approach is based on [24], where Hübel et al. model potassium dynamics during SDs. They proposed to take into account buffering mechanisms taking place at even slower timescales than the usual slow ion concentration *vs.* fast membrane potential separation. See for example Fig. 11 of [24].

System (3) is inspired by the FHN model [35, 20]. We wanted to have both a low (physiological) and a high (pathological) stable steady state for $[\text{K}]_o^+$, with a region of bistability and a threshold effect for the transition to the high state. System (3) allows us to obtain those elements (see Section 4) with only polynomial terms. The idea is to reproduce the initially slow increase of $[\text{K}]_o^+$ followed by a sharp rise, which is observed experimentally at the site of CSD initiation Fig. 1.

2.5 Potassium release

In addition to synaptic inhibition (see Section 2.3), another key aspect we retain from the biophysical model of [29] is the release of potassium by the neurons. Indeed, we concluded from our experimental [9] and simulation [29] results that activity-dependent accumulation of potassium plays a key role in CSD initiation.

We model the contribution of each neuron with a sigmoid function g of the voltage, which appears in Eq. (1e):

$$g(x) = g_K \frac{1}{1 + e^{-k_K(x - \theta_K)}}.$$

The intended effect is that each action potential increments $[\text{K}]_o^+$, similarly to what we obtained with the detailed model in Fig. 3 (C₁-C₃) of [29], to model the generated fluxes of K⁺ ions through voltage-gated channels. It allows us to model Na_V1.1 migraine mutations, see Section 2.6.

2.6 Na_V1.1 mutations

Since Na_V1.1 is mainly expressed in GABAergic neurons, we assume in our model that the pyramidal neuron is not affected by mutations of this channel and implement them only for the GABAergic neuron.

2.6.1 Migraine

In our simulations of the detailed model in [29], we observed that Na_V1.1 migraine mutations amplify the net potassium efflux at each action potential of the GABAergic neuron (Fig. 3 (C₁-C₃) of [29]). Based on this, for the migraine condition we scale $g(x_i)$ by $p = 4$ in Eq. (1e). This term represents the release of potassium by the GABAergic neuron (Section 2.5). In this way, we increase the increments of $[\text{K}]_o^+$ at each spike of the GABAergic neuron.

2.6.2 Epilepsy

In [29] (Fig. 10), both model simulations and experimental recordings on cortical slices from *Scn1a*^{+/-} mice suggest the same: Na_V1.1 loss of function renders GABAergic neurons more susceptible to depolarization block. This hypothesis is consistent with other recordings on *Scn1a*^{+/-} mice, see for example Fig. 5 of [46].

To obtain this effect in our phenomenological model, we reduce the value of the parameter c for the GABAergic neuron (parameter c_i in the full system). For the default parameter values ($c = 3$), the switch from repetitive firing to depolarization block occurs through a fold of limit cycle bifurcation at $I \approx 1.52$ (Fig. 4(a₁)). When we decrease the value of c to 1.2 (Fig. 4(a₂)), this transition happens via a supercritical Hopf bifurcation. Compared to the subcritical Hopf in Fig. 4(a₁), this Hopf bifurcation has been shifted to $I \approx 0.43$, see the 2-parameter bifurcation diagram in the (I, c) parameter plane in Fig. 4(b). What is most important here is not the fact that the transition to depolarization block is mediated by a different bifurcation, but rather that it can be triggered by much lower input values. Note that the saddle-node bifurcations are unaffected, since c does not influence the shape of the equilibrium branch. Reducing the value of c_i in the full system is thus a convenient way to model Na_V1.1 epileptogenic mutations.

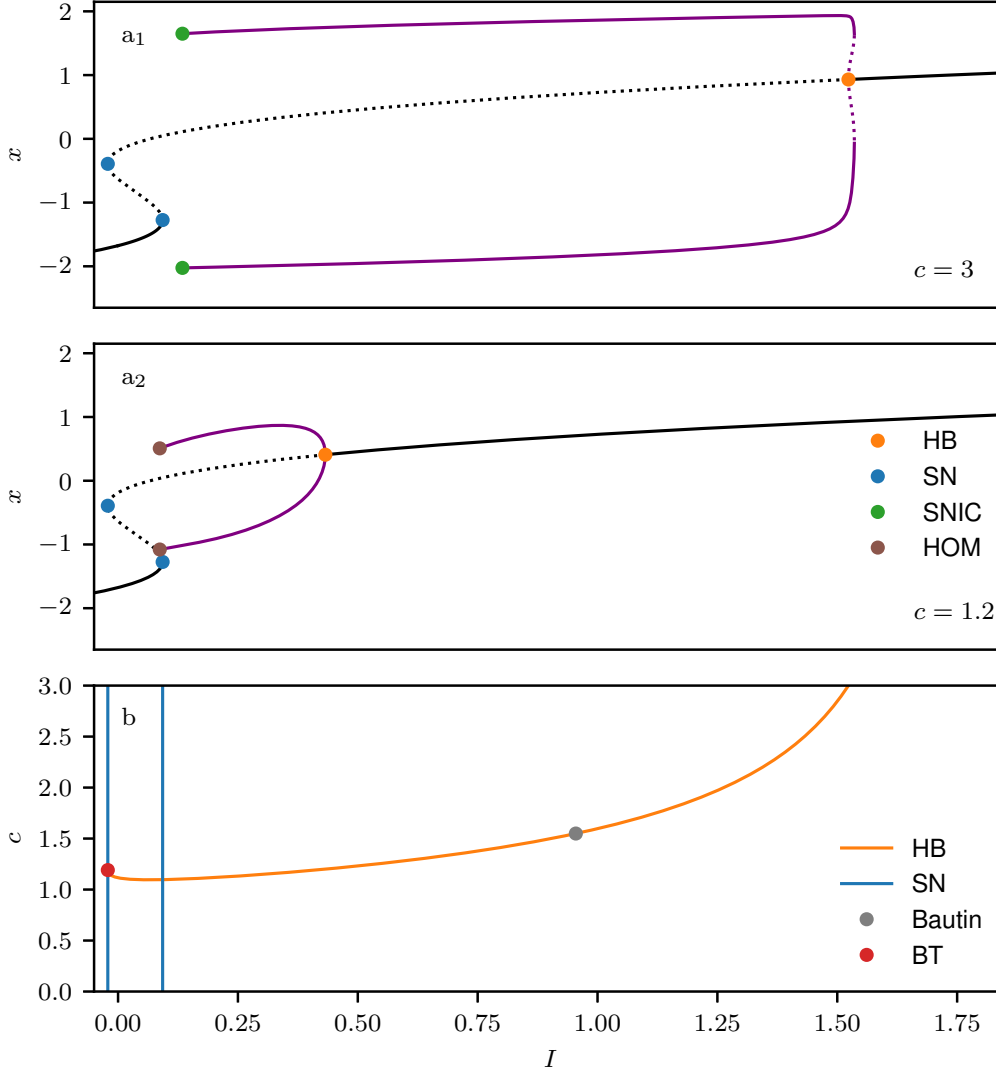


Figure 4: Modeling Nav1.1 epileptogenic mutations. (a₁) Bifurcation diagram x vs. I of System (2) for the default parameter values ($c = 3$: wild-type condition). (a₂) Bifurcation diagram when c is reduced to 1.2 to model Nav1.1 epilepsy mutations. The bifurcation corresponding to the transition to depolarization block (here supercritical Hopf) occurs at a much smaller value of I than in (a₁). HOM: homoclinic bifurcation. (b) 2-parameter bifurcation diagram in the (I, c) plane. At the Bautin bifurcation, the criticality of the Hopf changes, from subcritical (like in a₁) to supercritical (like in a₂). BT: Bogdanov-Takens bifurcation.

3 Fast dynamics

In this section we consider the fast layer problem, which is derived by taking the limit $\varepsilon \rightarrow 0$ in System (1):

$$\begin{aligned}
 \frac{dx_e}{dt} &= c_e \left(x_e - \frac{x_e^3}{3} - y_e + [\text{K}]_o^+ + I_{\text{ext}} - I_{\text{GABA}}(x_e, x_i) \right) \\
 \frac{dy_e}{dt} &= \frac{x_e^2 + dx_e - by_e + a}{c_e} \\
 \frac{dx_i}{dt} &= c_i \left(x_i - \frac{x_i^3}{3} - y_i + [\text{K}]_o^+ + I_{\text{ext}} \right) \\
 \frac{dy_i}{dt} &= \frac{x_i^2 + dx_i - by_i + a}{c_i}
 \end{aligned} \tag{4}$$

We are interested in the dynamics of the two neurons, which are coupled through the inhibitory current I_{GABA} , when the slow extracellular potassium $[\text{K}]_o^+$ is treated as a bifurcation parameter. We focus on the case where $I_{\text{ext}} = 0.35$, which is the value of external input we use in the simulations of the full system in Section 5. We computed the bifurcation diagram with respect to $[\text{K}]_o^+$ for $c_i = 3$, which corresponds to the wild-type and migraine conditions (Fig. 5), and when c_i is reduced to 1.2, to model the epilepsy mutation (Fig. 6).

In both cases, the bifurcation structure of the 4-dimensional system is much richer than that of a single neuron (Section 2.2 and Section 2.6). We find additional limit cycle bifurcations, such as a torus bifurcations (Fig. 5(a₁, b)

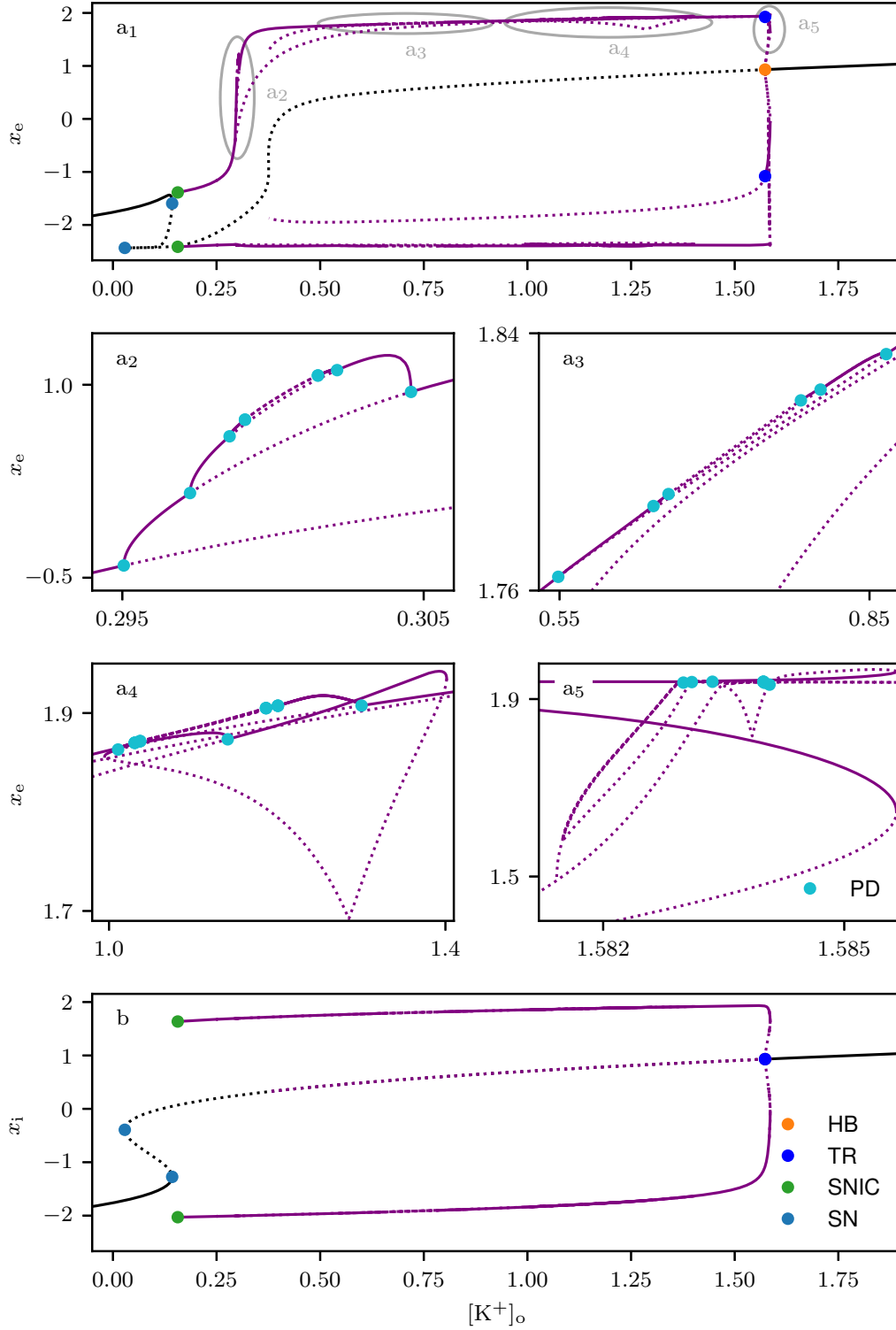


Figure 5: Dynamics of the fast layer problem in the wild-type and migraine conditions. Bifurcation diagram x_e vs. $[K^+]_o$ (a) and x_i vs. $[K^+]_o$ (b) of System (4) when $c_i = 3$, which corresponds to the wild-type and migraine conditions, for an external input $I_{ext} = 0.35$. (a2 - a5) Enlargements near the period-doubling bifurcations (PD). TR: torus bifurcation.

and Fig. 6 (a2)) and cascades of period-doubling bifurcations (Fig. 5 (a2 - a5) and Fig. 6 (a2)) which suggest regions of chaos. There are also isolas of limit cycles (Fig. 6 (a2)), which often arise in multi-timescale systems displaying complex oscillations [12, 41, 28]. It is not possible to give a direct biological interpretation for each of those. The essential point is that the key features which we need to model Nav1.1 mutations are preserved from Fig. 4 (a1) and Fig. 4 (a2).

Note that the coupling between the two neurons is unidirectional: the pyramidal neuron has no influence on the GABAergic neuron (Fig. 2). The dynamics of (x_i, y_i) in the fast layer problem is thus exactly as in the two-dimensional case of Eq. (2).

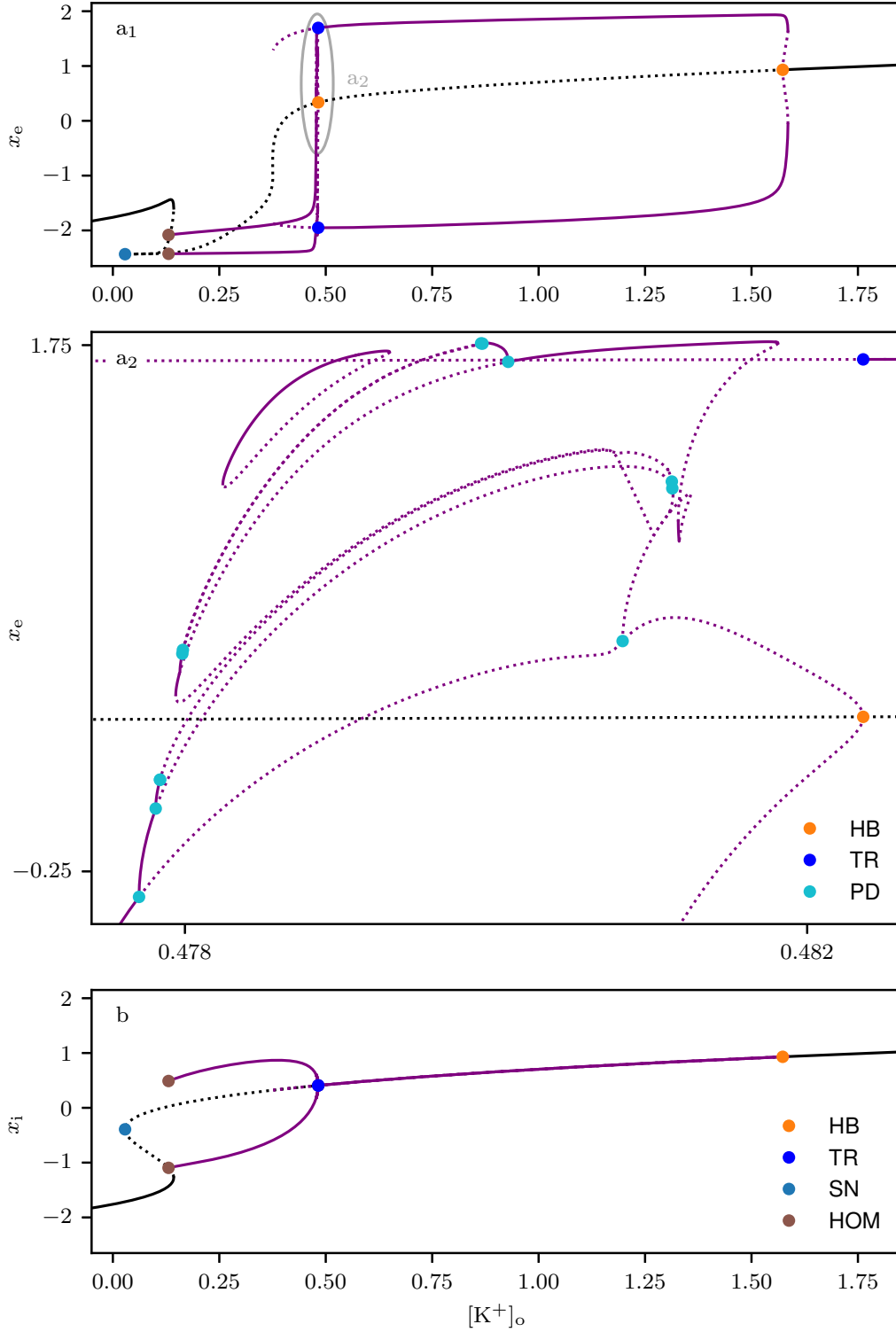


Figure 6: Dynamics of the fast layer problem in the epilepsy condition. Bifurcation diagram x_e vs. $[K^+]_o^+$ (a) and x_i vs. $[K^+]_o^+$ (b) of System (4) when $c_i = 1.2$, which corresponds to the epilepsy condition, for an external input $I_{\text{ext}} = 0.35$.

3.1 Migraine vs. wild-type condition

In Fig. 5, we can identify four main activity regimes for the pair of neurons, depending on the extracellular potassium concentration:

1. For very low $[K^+]_o^+$ up to the SNIC bifurcation, both neurons are at rest.
2. For $[K^+]_o^+$ beyond the SNIC up to approximately 0.28, the system converges to limit cycles that are of large amplitude for the GABAergic neuron, corresponding to tonic firing, but of low amplitude for the pyramidal neuron. This behavior, which we interpret as aborted spikes, is due to the inhibitory current I_{GABA} at each spike of the GABAergic neuron.
3. For $[K^+]_o^+$ between approximately 0.31 and 1.57, the only stable objects are limit cycles of large amplitude for both

neurons. This interval comprises the range of $[K]_o^+$ values on the branch of physiological stable equilibria of the potassium block (3) (Fig. 7). Interestingly, the period-doubling bifurcations allow here for more complex spiking patterns for the pyramidal neuron than in the single neuron case (Fig. 4(a₁)), with aborted action potentials and varied spike shapes along a train of action potentials. This is consistent with simulations of the detailed model, see for example the voltage traces in Fig. 4 of [29].

4. For $[K]_o^+$ beyond 1.59, the only attractor is a stable equilibrium with high $x_{e,i}$ values. A too large rise of $[K]_o^+$ would thus provoke the transition to depolarization block of both neurons, as we will see in the migraine case in Section 5.1.

3.2 Epilepsy condition

In the wild-type case (Fig. 5), the Hopf bifurcation which occurs at a high value of $[K]_o^+$ is in fact a double Hopf [22]: the two pairs of complex conjugate eigenvalues cross the imaginary axes of the complex plane at the same time. To model the epilepsy mutations, we decreased c_i to 1.2 for the GABAergic neuron while keeping $c_i = 3$ for the pyramidal neuron. As a consequence, the double Hopf splits into two: H_L at $[K]_o^+ = K_L \approx 0.482$ and H_U at $[K]_o^+ = K_U \approx 1.573$ (Fig. 6). When crossing H_L from $[K]_o^+ < K_L$ to $[K]_o^+ > K_L$, the real part of one of the pairs of eigenvalue becomes negative: the branch of unstable foci remains unstable but gains two stable directions. At H_U , the branch of equilibria stabilizes as the real part of the two other eigenvalues also becomes negative.

The bifurcation structure in the narrow region ($0.477 < [K]_o^+ < 0.483$) near H_L is complicated (Fig. 6(a₂)). H_L gives rise to a branch of limit cycles and we found isolas, which we computed by continuation starting from stable complex solutions obtained by direct simulation. Both undergo cascades of period-doubling bifurcations. Before this narrow region ($[K]_o^+ < 0.477$), there is a branch of limit cycles which corresponds to aborted spikes of the pyramidal neuron and firing of the GABAergic neuron. On the other side ($[K]_o^+ > 0.483$), there is a branch of stable limit cycles for which the pyramidal neuron spikes but the GABAergic neuron is at steady state.

In fact, we suspect that the torus bifurcation which stabilizes this branch of limit cycles occurs at the same value of $[K]_o^+$ as the Hopf bifurcation H_L . Without providing a rigorous proof, an important element appears to be the unilateral forcing from the GABAergic neuron to the pyramidal one. For $[K]_o^+ > K_L$, the (x_i, y_i) component of the stable limit cycles is stationary, because the dynamics of the GABAergic neuron cannot be different than in the two-dimensional case. At H_L , limit cycles of small amplitude emerge, which are stable for (x_i, y_i) . When the forcing I_{GABA} onto the pyramidal neuron becomes periodic, it must cause a qualitative change to the relaxation cycles of (x_e, y_e) , which is compatible with a torus bifurcation. A similar reasoning can be applied in the case of Fig. 5, where the torus bifurcation occurs at the same value of $[K]_o^+$ as the double Hopf, although the criticality of the Hopf is different.

What interests us in this bifurcation structure is the possibility of depolarization block of the GABAergic neuron for low concentrations of potassium, when the external input is strong enough (here $I_{ext} = 0.35$). It was not the case in the wild-type condition (Fig. 5). As we mentioned before, the dynamics of (x_i, y_i) in the fast layer problem is unchanged compared to Eq. (2). The enhanced susceptibility of the GABAergic neuron to depolarization block is thus achieved here in exactly the same way as in the two-dimensional system (Fig. 4), namely by shifting the Hopf bifurcation for the GABAergic neuron to lower values of potassium or external inputs (Fig. 4).

4 Slow dynamics

We analyze now the flow of the slow and superslow variables, $[K]_o^+$ and w , respectively.

4.1 Potassium dynamics for a constant efflux g_{tot} from the neurons

We consider first the simplified case where the flux of potassium from the neurons into the extracellular space is constant. We study thus the system

$$\begin{aligned} \frac{d[K]_o^+}{dt} &= w - f([K]_o^+) + g_{tot} \\ \frac{dw}{dt} &= \delta(-[K]_o^+ - \alpha + \beta w) \end{aligned} \quad (3)$$

where g_{tot} is a parameter. Fig. 7 shows its bifurcation diagram with respect to g_{tot} . The lower branch of stable equilibria in Fig. 7 corresponds to physiological levels of extracellular potassium while the upper one corresponds to pathological states. When the neurons release too much potassium, only the pathological state remains, but before this threshold, there is a range of positive values of g_{tot} for which the two states coexist.

To investigate the dynamics in this zone of bistability, we calculated the phase portrait of System (3) for two nearby values of g_{tot} (Fig. 8). At the intersection of the nullclines, we can see the two stable equilibria and a saddle point between them, much closer to the lower equilibrium. The stable invariant manifold of this saddle acts as a threshold: it defines the boundary between the basins of attraction of the two attractors. This threshold is sensitive to variations

of g_{tot} . To illustrate this effect, we plotted in purple two trajectories from the same initial condition for the two values of g_{tot} . Even though they are very close, the outcome is completely different. For $g_{\text{tot}} = 0.0074$, the system converges to the physiological equilibrium while for $g_{\text{tot}} = 0.0075$ it converges to the pathological one.

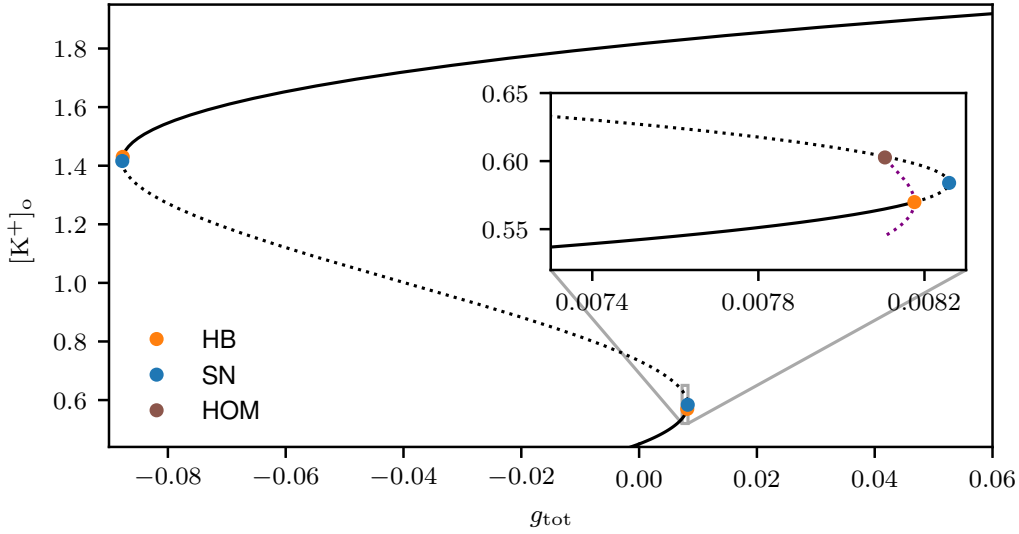


Figure 7: Bifurcation diagram $[K]_o^+$ vs. g_{tot} of System (3). We represented steady states with black lines and limit cycles with purple lines. In the full system (1) the contribution of neuronal firing to extracellular potassium concentration $pg(x_i) + g(x_e)$ is positive, so only positive values of g_{tot} are relevant here.

Note that the potassium block is itself a slow-fast system; its timescale separation is organized by the parameter δ . When δ is at its default value ($\delta = 0.005$), $[K]_o^+$ is faster than w . The sensitivity of the stable manifold of the saddle is preserved even when increasing δ beyond the point where the roles of the two variables are exchanged, w becoming faster than $[K]_o^+$. This is for example the case for $\delta = 1$. Regarding this aspect, having three timescales (superslow, slow and fast) in the full system is not crucial for modeling the jump to the high potassium state. However, we noticed that a small value of δ is necessary to obtain an overshoot in the trace of $[K]_o^+$ before convergence to the upper equilibrium. Such an overshoot is consistent with the experimental trace of Fig. 1. When $[K]_o^+$ is the fast variable of the potassium block, the trajectory is almost horizontal until the cubic nullcline, before moving down slowly along it (dashed purple line in Fig. 8 (a)). This shapes the overshoot. On the other hand, when w is the fast variable, the trajectory converges to the upper equilibrium along the w -nullcline, which does not produce any overshoot (not shown).

4.2 Potassium dynamics averaged over one steady state cycle of the fast layer problem

In the previous section, we showed that for larger, constant, efflux of potassium from the neurons, the basin of attraction of the low- $[K]_o^+$ stable equilibrium diminishes until only the high- $[K]_o^+$ stable equilibrium remains. We are now interested in how neuronal activity can dynamically drive $[K]_o^+$ to the high state. When the neurons are spiking, $[K]_o^+$ is perturbed by increments associated with each action potential. This discontinuous release is modeled in the full system (1) by the term $g_{\text{tot}} = pg(x_i) + g(x_e)$, which oscillates rapidly (see Fig. 10 (a₅, b₅, c₅)). Those oscillations are so fast compared to the slow variables ($[K]_o^+$, w), that their response is governed by the average value of g_{tot} , as we will illustrate in Fig. 13 (c).

To eliminate the fast spiking dynamics, we base ourselves on the averaging method, which is commonly employed when modeling ion concentration dynamics [11, 44, 4]. We formulate the following reduced system, in which the derivatives of the slow variables (Eqs. (1e) and (1f)) are averaged over one period T of the steady state oscillation of the fast layer problem:

$$\begin{aligned} \frac{d[K]_o^+}{dt} &= w - f([K]_o^+) + \overline{g_{\text{tot},\infty}}([K]_o^+), \\ \frac{dw}{dt} &= \delta(-[K]_o^+ - \alpha + \beta w), \end{aligned} \quad (4)$$

where

$$\begin{aligned} \overline{g_{\text{tot},\infty}} &= p\overline{g_{i,\infty}} + \overline{g_{e,\infty}} \\ &= \frac{1}{T([K]_o^+)} \left(p \int_0^{T([K]_o^+)} g(x_i(\tau, [K]_o^+)) d\tau + \int_0^{T([K]_o^+)} g(x_e(\tau, [K]_o^+)) d\tau \right). \end{aligned}$$

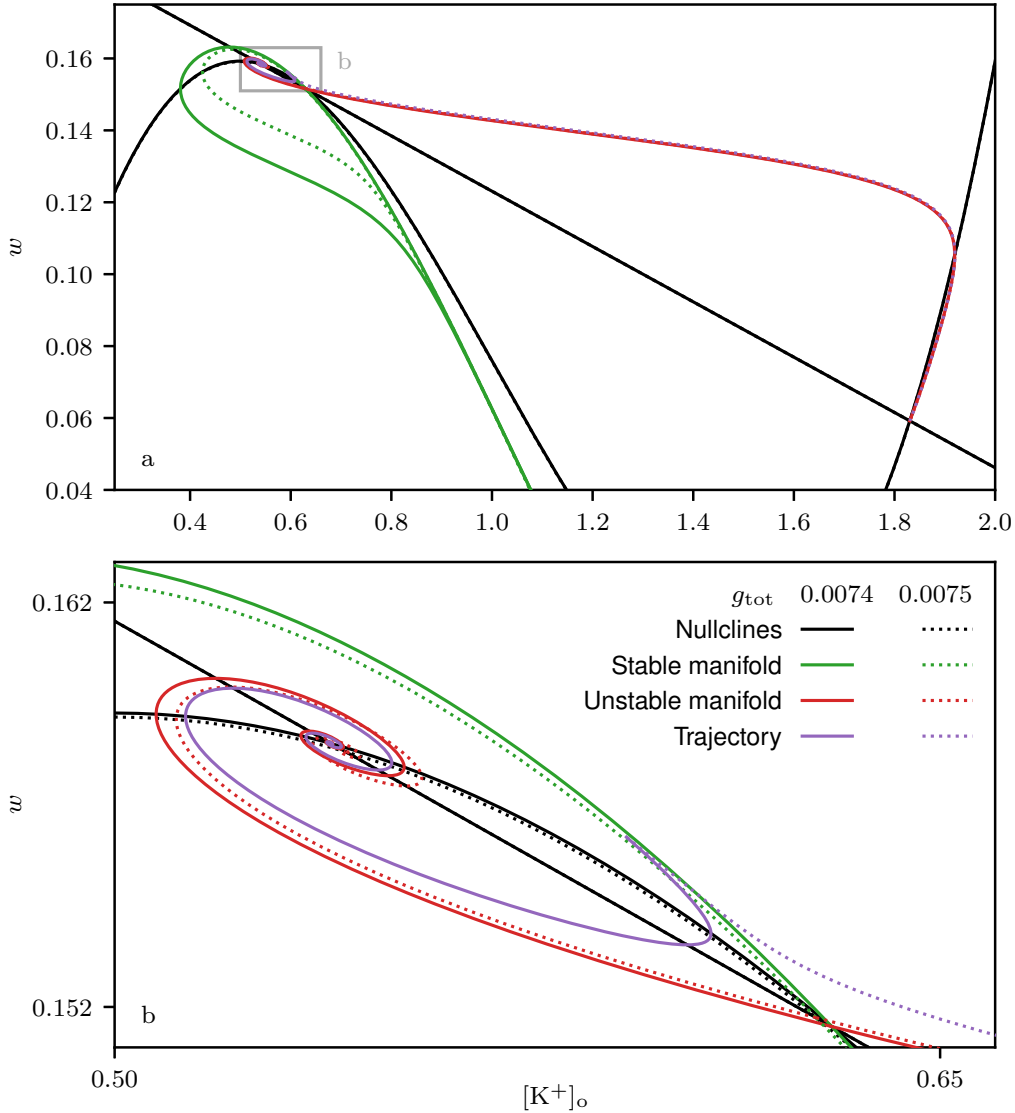


Figure 8: Phase portrait of System (3) for two close values of g_{tot} in the zone of bistability. In both cases there are two stable equilibria, whose basins of attraction are delimited by the stable invariant manifold of a saddle. We show trajectories from the same initial condition for both values of g_{tot} . For $g_{\text{tot}} = 0.0074$, the system converges to the low- $[\text{K}]_o^+$ stable equilibria (solid purple line). For $g_{\text{tot}} = 0.0075$, it converges to the high- $[\text{K}]_o^+$ stable equilibria (dashed purple line, visible closely above the unstable manifold in panel a, and at the bottom right of panel b).

We then replace $\overline{g_{i,\infty}}$ and $\overline{g_{e,\infty}}$ with fitted functions of $[\text{K}]_o^+$ (Fig. 9(a)), a simplification similar to the one used by Cressman et al. in [11]. We perform those fits in the region of interest $[\text{K}]_o^+ \in (0.31, 0.95)$, in which there is a unique stable limit cycle of the fast layer problem for a given $[\text{K}]_o^+$.

Fig. 9(b) shows the bifurcation diagram of the resulting system with respect to the parameter p , which represents the severity of $\text{Na}_V1.1$ migraine mutation. When p is too high, there is no low- $[\text{K}]_o^+$ stable equilibrium (Fig. 9(c₃)). Before that, when both stable equilibria coexist (there is a high- $[\text{K}]_o^+$ stable equilibrium outside of the range of $[\text{K}]_o^+$ values shown here), the behavior depends on the basin of attraction the initial conditions lie in. The basin of attraction of the low stable equilibria, bounded by the stable invariant manifold of the saddle, is reduced when p is increased from its default value $p = 1$ (Fig. 9(c₁, c₂)). As a consequence, smaller perturbations can trigger the increase of extracellular potassium to pathological concentrations.

5 Full system

Finally, we examine the dynamics of the full system (1). We compare the configurations: wild-type, migraine and epileptogenic mutation of $\text{Na}_V1.1$ (see Section 2.6). Fig. 10 shows trajectories of the system in the three cases, when the neurons are stimulated with an external input $I_{\text{ext}} = 0.35$. To understand how the different responses are produced, we look at the superposition of the full system's trajectories onto the bifurcation diagram of the fast layer problem with respect to $[\text{K}]_o^+$. This procedure of slow-fast dissection is a classical tool to study multiple-timescale systems and was introduced by J. Rinzel, see for instance [39].

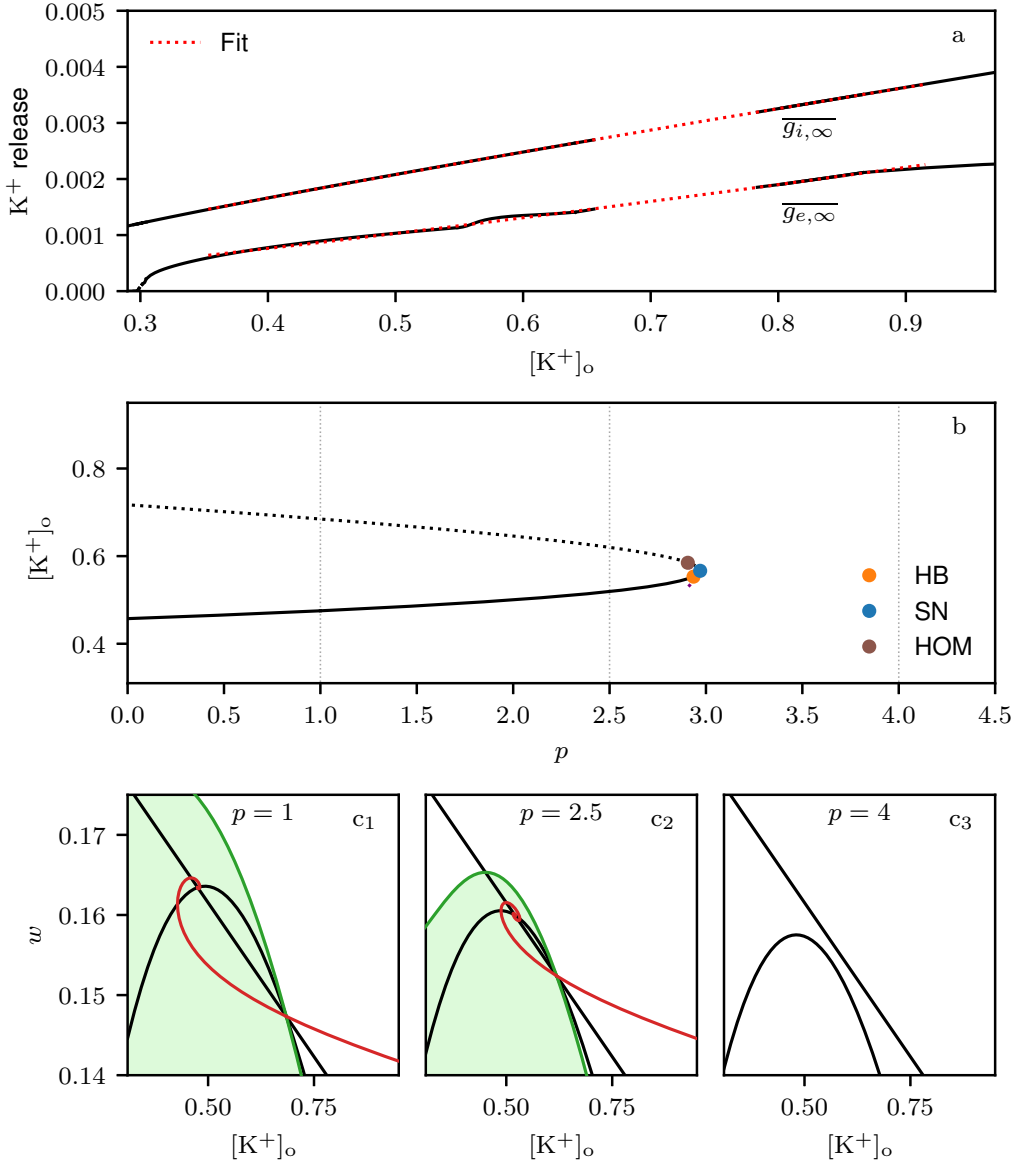


Figure 9: Approximated average slow subsystem. (a). Potassium efflux from the GABAergic ($g(x_i)$) and pyramidal ($g(x_e)$) neurons on the stable limit cycle of the fast layer problem, averaged over one period. Dashed red lines: fit of those with a power function. (b) Bifurcation diagram $[K^+]_o$ vs. p and (c) phase portraits of System (4), in which $\overline{g_{i,\infty}}$ and $\overline{g_{e,\infty}}$ have been replaced by the corresponding fitted function.

5.1 The route to CSD initiation

In the absence of mutation, extracellular potassium remains at low concentrations, for which the neurons are in a firing regime (Fig. 10(a), Fig. 11).

With the migraine mutations, neuronal activity releases by construction more potassium (Fig. 10(b₅) vs. Fig. 10(a₅)). It accumulates progressively, until a “tipping point” is reached, resulting in an abrupt transition to the high state (Fig. 10(b₃)) with a slight overshoot. This progression is consistent with what is measured experimentally (Fig. 1). As $[K^+]_o^+$ increases, the voltage traces show a good agreement with the bifurcation diagram of the fast layer problem (Fig. 12). Meanwhile, the firing frequency of the neurons increases considerably (Fig. 10(b₁, b₂)), similarly to simulations of the detailed model (Fig. 5 (e, f) of [29]) and experiments (Fig. 5 (a, b) of [29]). Note that the frequency of the limit cycles in Fig. 11 is not necessarily the firing frequency: there can be more than one full blown action potential per period, due to period-doubling bifurcations. The switch from the spiking regime to depolarization block of the two neurons, which indicates CSD initiation, is achieved via a *dynamic bifurcation* of limit cycles. It is unclear which is the precise bifurcation responsible for this transition, since there are several branches of limit cycles in this region (Fig. 5(a₅)) and $[K^+]_o^+$ is undergoing a relatively fast increase. The key point is that $[K^+]_o^+$ reaches values for which the depolarized steady state is the only attractor.

We took a closer look at the threshold between physiological and pathological responses. In Fig. 13, two very close values of p lead to either regular spiking or depolarization block of the neurons. We can see in the inset of Fig. 13(a) the critical moment where the two potassium traces separate (blue and orange curves). While $[K^+]_o^+$ builds up, the

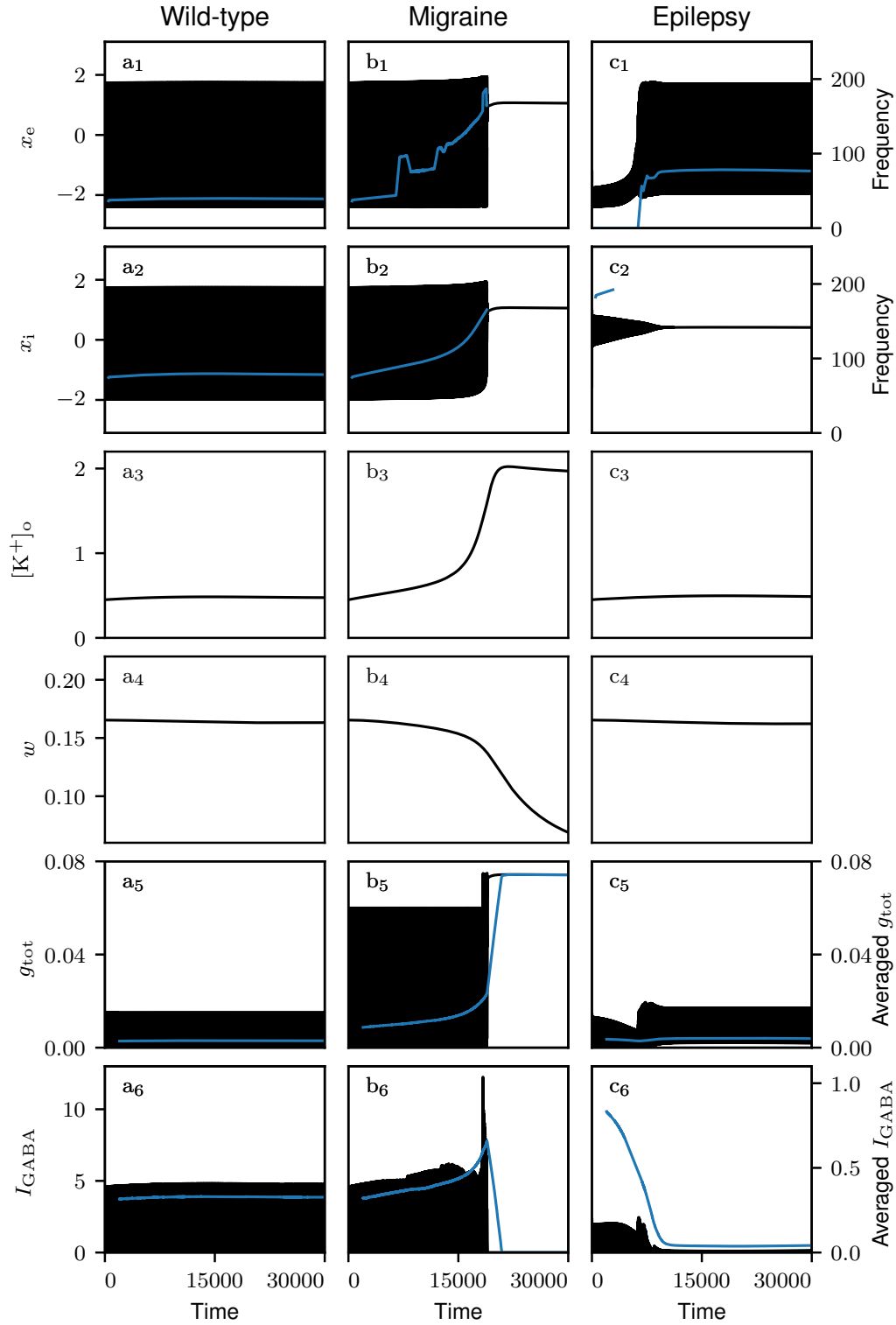


Figure 10: Trajectories of the full system (1). Time traces for an external input $I_{ext} = 0.35$, taking as initial condition the steady state when $I_{ext} = 0$. We represented in blue the firing frequency of the neurons averaged on a sliding window of 500 time units. In the last two rows, we plotted the contribution g_{tot} of neuronal spiking to the extracellular potassium and the inhibitory current I_{GABA} (black curves), together with their average on a sliding window of 2000 time units (blue curves). (a) Wild type condition: default parameter values. (b) Migraine condition: $p = 4$. (c) Epilepsy condition: $c_i = 1.2$.

contribution g_{tot} of neuronal firing to $[\text{K}]_o^+$ increases as well (Fig. 13 (b)), which creates a positive feedback loop. In Fig. 13 (c), we projected those trajectories onto the $([\text{K}]_o^+, w)$ plane, where for each value of p we also represented the phase portrait of the approximated average slow subsystem (System (4) with fitted $\overline{g_{i,\infty}}$ and $\overline{g_{e,\infty}}$). In both cases, the full system first approaches the saddle along its stable invariant manifold, before either abruptly ascending to high potassium concentrations, or converging to the low- $[\text{K}]_o^+$ stable equilibrium. The outcome depends on the relative position of the initial condition with respect to the stable invariant manifold (see insets), which is a validation of our averaging procedure.

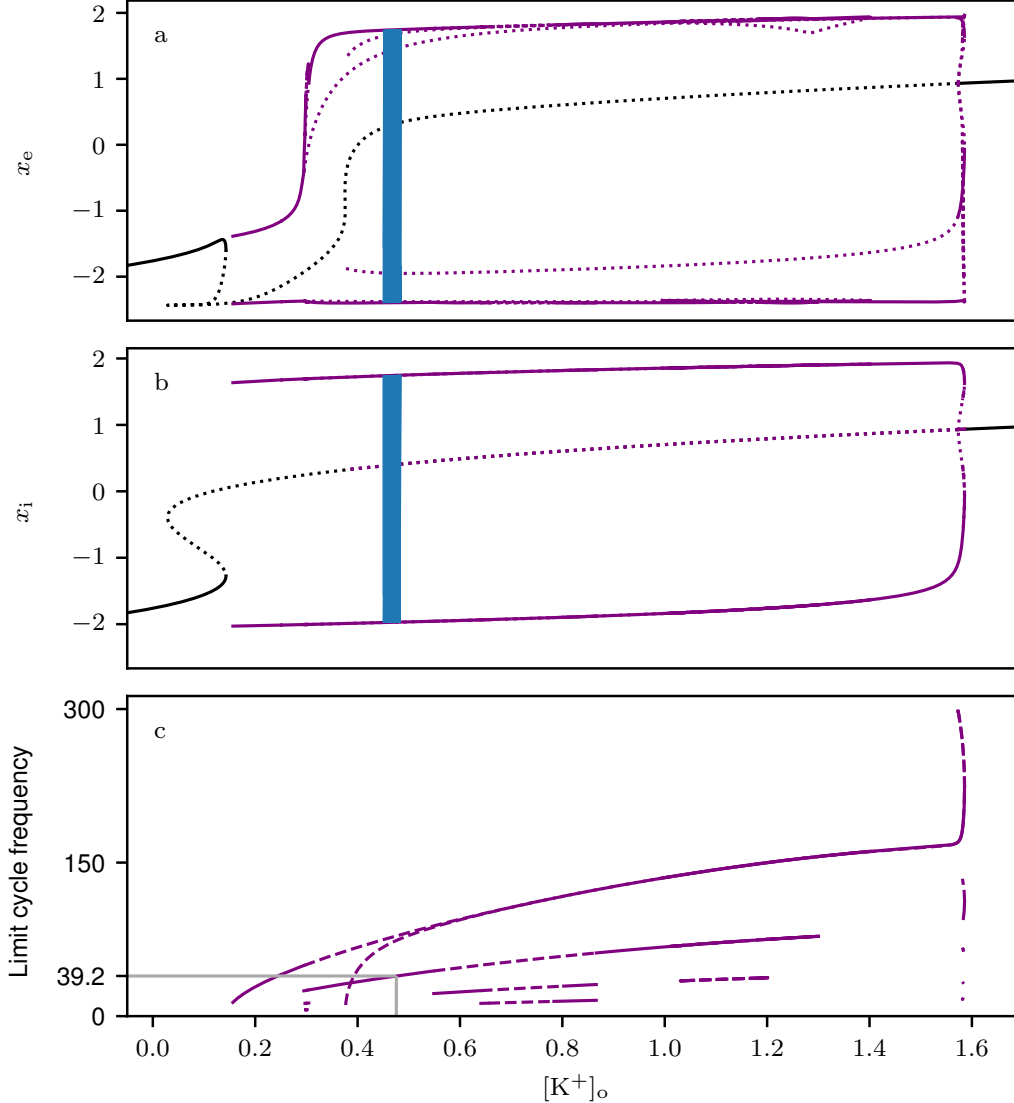


Figure 11: Wild-type condition: tonic firing of the neurons. We superimposed the trajectories of the full system shown in Fig. 10 (a) onto the bifurcation diagram of the fast layer problem (4) for $c_3 = 3$. (a) Voltage of the pyramidal neuron x_e vs. $[\text{K}]_o^+$. (b) Voltage of the GABAergic neuron x_i vs. $[\text{K}]_o^+$. (c) Frequency of the limit cycles. We marked in gray the final $[\text{K}]_o^+$ value of the full system trajectory.

5.2 The route to pre-epileptic hyperactivity

With the epileptogenic mutations, the system first follows the branch of limit cycles for which the pyramidal neuron produces aborted spikes while the amplitude of the GABAergic neuron's action potentials diminishes (Fig. 14). Shortly after surpassing the low Hopf bifurcation H_L , the GABAergic neuron enters depolarization block, with a delay due to the speed of $[\text{K}]_o^+$. This causes a drop of the inhibitory current (Fig. 10 (c₂, c₆)). Consequently, the pyramidal neuron starts spiking at high frequency compared to the wild-type case (Fig. 10 (c₁) vs. Fig. 10 (a₁)), which we interpret as pre-epileptic hyperactivity. In this simulation the extracellular potassium concentration remains low. Note that during a full blown seizure, which is not what we aim to model here, one would expect a larger increase in extracellular potassium. The limit firing frequency is almost twice as high as for the wild-type case (Fig. 11 (c) vs. Fig. 14 (c)). In those particular cases, the frequency of the limit cycles corresponds to the firing frequency, since only one action potential is emitted per period.

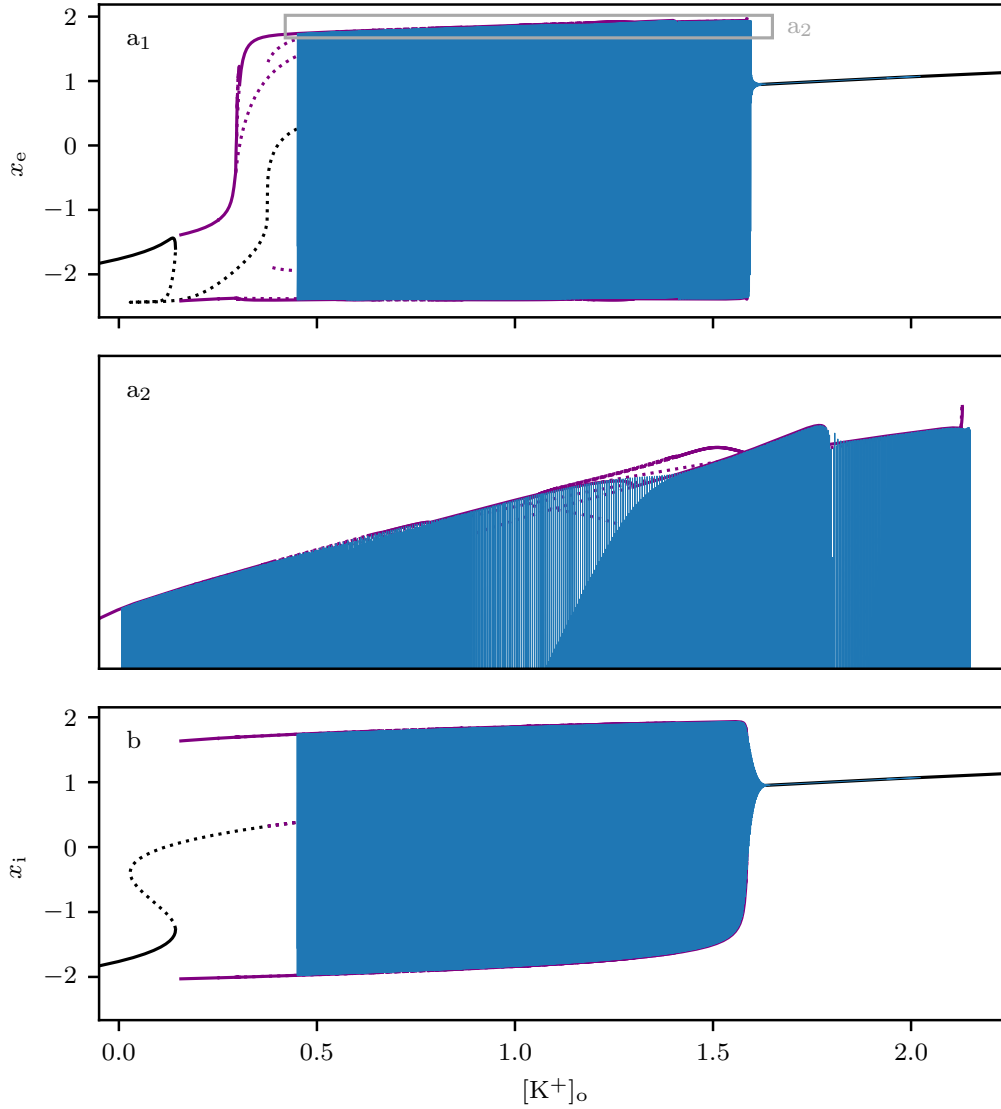


Figure 12: Migraine condition: depolarization block of the two neurons. We superimposed the trajectories of the full system shown in Fig. 10 (b) onto the bifurcation diagram of the fast layer problem (4) for $c_i = 3$. (a) Voltage of the pyramidal neuron x_e vs. $[K^+]_o^+$. (b) Voltage of the GABAergic neuron x_i vs. $[K^+]_o^+$.

What exactly happens at the transition between the two phases for the pyramidal neuron is not straightforward, as the bifurcation landscape is very intricate (Fig. 6 (a₂)). One way to address this would be to study the dynamics closer to the singular limit by reducing ε and observing which branches play a role for the full dynamics.

6 Conclusion and perspectives

In this paper, we have designed and analyzed a reduced version of our biophysical model [29] of CSD initiation and epileptiform hyperactivity. We constructed this six-dimensional system to mirror the microcircuit structure of the detailed model. Namely, we considered two coupled idealized neurons, a pyramidal cell and a GABAergic neuron that inhibits it, and additional variables to model the dynamics of extracellular potassium, which is the most relevant ion concentration in this context. Albeit phenomenological in spirit, with mostly polynomial terms and mathematical excitable models for its three blocks — 2D Hindmarsh-Rose type model for each neuron, FitzHugh-Nagumo (FHN) type model for the potassium —, this reduced model still retains salient features of the biophysical model, in the form of the inhibitory synaptic current and the function governing potassium release. In this simpler setting, we managed to reproduce both pathological transitions upon minimal parameter variation: one parameter for each scenario. We exploited the minimal structure of the model, as well as its explicit timescales, to identify dynamical mechanisms underpinning the two pathological transitions. Those mechanisms are robust, in the sense that the only requirement on the parameter choice is to obtain the suitable bifurcation structure in the fast subsystem and phase-space structure of the slow block. Many parameter sets will offer such configuration. Now, the transition from a tonic firing scenario to CSD-like dynamics with a depolarization block is very sensitive to parameter variation, as it is the result of the interaction between multiple timescales and the underlying excitable structure of the slow block. This is illustrated in

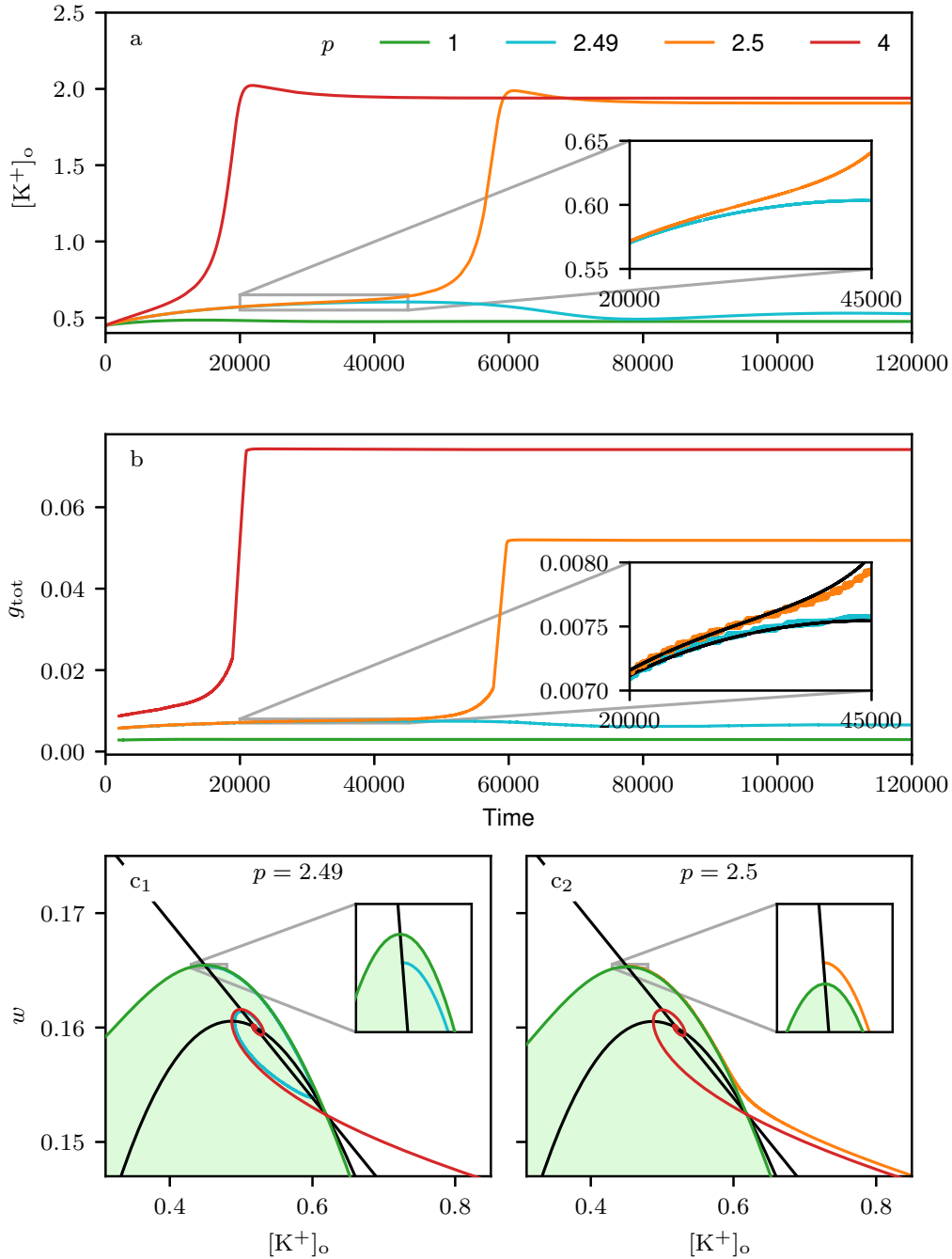


Figure 13: Activity-mediated jump of the extracellular potassium to pathological elevated concentrations. Simulations of the full system (1) for an external input $I_{ext} = 0.35$ and for different values of the parameter p , which controls the release of potassium by the GABAergic neuron. (a) Extracellular potassium. (b) Total contribution of neuronal firing to the extracellular potassium, averaged on a sliding window of 2000 time units. (c) Projection of the full system trajectories onto the $([K^+]_o, w)$ plane, where the phase portrait of an approximation of the two-dimensional System (4) is also depicted, for (c₁) $p = 2.49$ and (c₂) $p = 2.5$.

Fig. 13, where for two close values of p the trajectories are very different.

One important novelty of our model is the possibility to capture the abrupt increase of extracellular potassium in the CSD scenario, with an overshoot at the beginning of the depolarization block phase. To this end, we introduced a third timescale and hence modeled the potassium dynamics with two variables, inspiring from [24]. With this approach the potassium block is a bistable slow-fast system, whose unstable (saddle) equilibrium organizes the transition to depolarization block via its stable manifold. As we indicated in Section 4, getting rid of the third timescale maintains the sharp transition to the high potassium state, but without the overshoot that we observed in the experimental data. We showed that analyzing the planar potassium system, in particular the dependence of the stable separatrix of the saddle upon neuronal feedback, is enough to grasp the mechanism of CSD initiation in the full system.

In the case of $Na_V1.1$ epileptogenic mutations, we have shown that the main ingredient is a shift in the position of a Hopf bifurcation in the fast layer problem, obtained by continuing in two parametric dimensions the corresponding

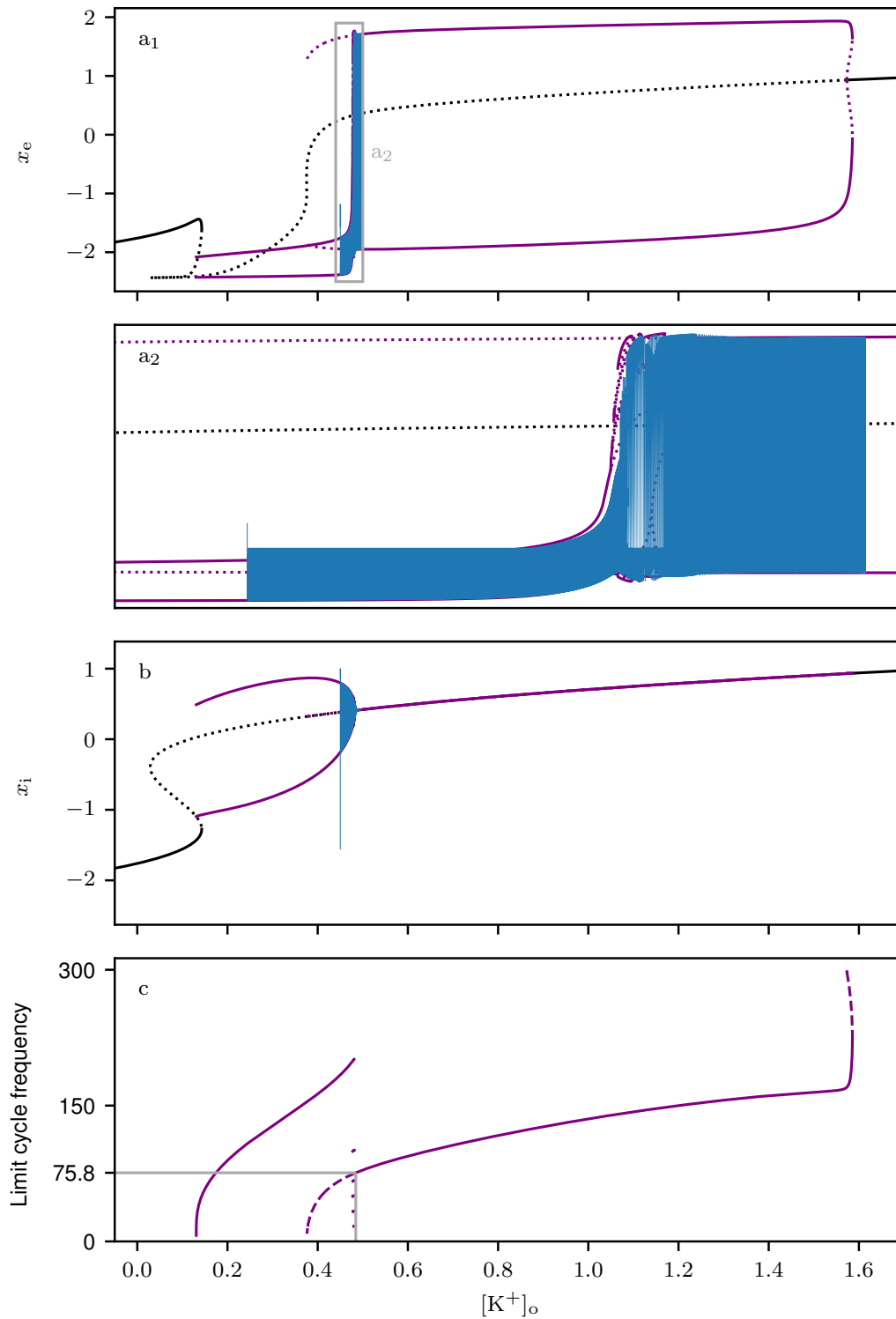


Figure 14: Epilepsy condition: depolarization block of the GABAergic neuron and high firing frequency of the pyramidal neuron. We superimposed the trajectories of the full system shown in Fig. 10(c) onto the bifurcation diagram of the fast layer problem (4) for $c_i = 1.2$. (a) Voltage of the pyramidal neuron x_e vs. $[K^+]_o$. (b) Voltage of the GABAergic neuron x_i vs. $[K^+]_o$. (c) Frequency of the limit cycles. We marked in gray the final $[K^+]_o$ value of the full system trajectory.

Hopf in the GABAergic neuron model. By varying one parameter in the full system, we reproduce the hypothesized biophysical mechanism: the GABAergic neuron enters depolarization block at low potassium level when the stimulation is strong enough, hence ceasing to inhibit, which induces an increase of the pyramidal neuron’s firing frequency.

Overall, this model is very similar in terms of its dynamical behavior to the much larger and nonlinear biophysical model developed and studied in [29]. An interesting avenue for future work would be to exploit the results reported in this paper to better understand the biophysical model and possibly improve it.

6.1 Towards simpler models

In future projects, the simplification of the model performed here could be taken further, facilitating a more advanced mathematical analysis. With a very basic model, we could also consider more than two neurons: this would allow us to take into account network effects involved in the initiation of CSD and seizures or even to study the propagation of these phenomena.

6.1.1 Extracellular potassium dynamics

Extracellular potassium is crucial for CSD initiation. The modeling of its dynamics in this work is already phenomenological (Section 2.4). To simplify it further, we could choose to use only one equation instead of a two-dimensional system. The minimal setup which we need is two stable steady states separated by a threshold. It could be achieved with an equation such as:

$$\frac{d[K]_o^+}{dt} = (K_1 - [K]_o^+)([K]_o^+ - K_2)([K]_o^+ - K_3), \quad 0 < K_1 < K_2 < K_3.$$

The stable equilibrium K_1 corresponds to a physiological level of potassium. An increase above the unstable equilibrium K_2 , chosen closer to K_1 than to K_3 , would cause a jump to the pathological stable equilibrium K_3 . The analogous of K_2 in the present model is the stable manifold of the saddle (Fig. 8), which delimits the basins of attraction of the two stable steady states.

One drawback of this approach is that $[K]_o^+$ cannot oscillate, preventing the trajectory to the high state to exhibit an overshoot. With this simplification, we would also lose the biological interpretation related to the slow buffering of extracellular ions of the two-dimensional slow-fast framework [24].

6.1.2 Neuronal dynamics

Transition to depolarization block is at the center of the pathophysiology of migraine with aura, and our work suggests that it might also be involved in the onset of seizures. As they are, computationally inexpensive models such as the theta model [18] cannot reproduce this pathological behavior. An interesting project would be to extend one of those simple models such that the neuron enters depolarization block when excessively stimulated. The motivation behind it is to build networks.

In the theta neuron, the transition from quiescence to repetitive firing occurs at a SNIC. For the extension mentioned above, we would need an additional bifurcation to mediate the transition from repetitive firing to depolarization block. The following example illustrates this idea:

$$\frac{d\theta}{dt} = (I - \cos\theta)(\cos\theta + I_{DB} + 1 - I), \quad \theta \in S^1. \quad (5)$$

A branch of stable limit cycles emerges through a SNIC at $I = 1$ and terminates at another SNIC at $I = I_{DB}$. If we define the voltage $v = \sin(\theta)$, the branch of stable equilibria created by the second SNIC corresponds to higher voltage values than the subthreshold branch (Fig. 15).

In a framework similar to Eq. (5), if extracellular potassium participates to the input I , a too large accumulation of this ion would cause depolarization block of the neuron (Fig. 15(B)), reproducing the mechanism of CSD initiation and possibly CSD propagation. To model the epilepsy condition, one could reduce the input value at which the transition to depolarization block occurs (here controlled by the parameter I_{DB}). Having a SNIC as spike-terminating bifurcation is not ideal: it means that the firing frequency tends to zero when converging to it. This is however not too problematic in the case of CSD, since the potassium input would not grow linearly, but instead rise relatively fast across the SNIC.

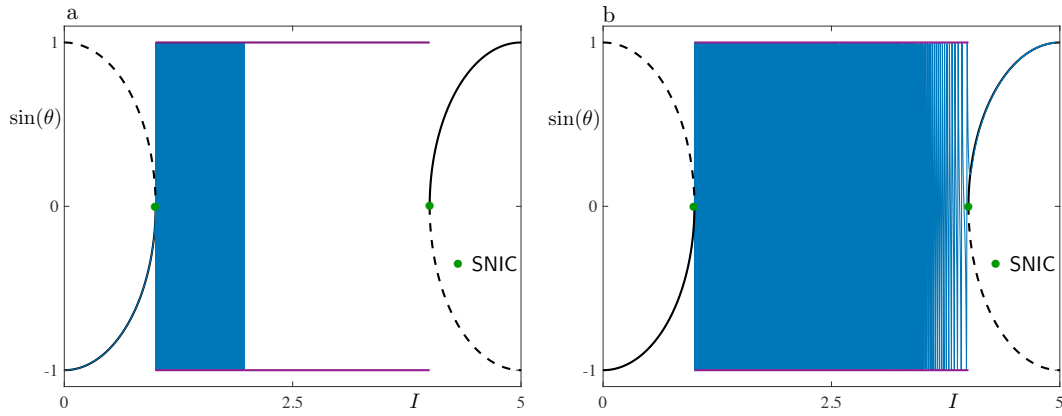


Figure 15: Depolarization block in a phase oscillator model. Bifurcation diagram $\sin(\theta)$ vs. I of Eq. (5) and superposition of trajectories when I slowly increases from 0 to 1.97 (a) or to 5 (b).

Acknowledgments

This research was funded by UCAJEDI (<https://univ-cotedazur.fr/ucajedi-lidex-duniversite-cote-dazur>, ANR-15-IDEX-01) and Laboratory of Excellence “Ion Channel Science and Therapeutics” - LabEx ICST (<https://www.labex-icst.fr/en>, ANR-11-LABX-0015-01).

References

- [1] Yael Almog, Anat Mavashov, Marina Brusel, and Moran Rubinstein. Functional Investigation of a Neuronal Microcircuit in the CA1 Area of the Hippocampus Reveals Synaptic Dysfunction in Dravet Syndrome Mice. *Frontiers in Molecular Neuroscience*, 15:823640, March 2022.
- [2] Eva Aufferberg, Ulrike B. S. Hedrich, Raffaella Barbieri, Daniela Miely, Bernhard Groschup, Thomas V. Wuttke, Niklas Vogel, Philipp Lühns, Ilaria Zanardi, Sara Bertelli, Nadine Spielmann, Valerie Gailus-Durner, Helmut Fuchs, Martin Hrabě de Angelis, Michael Pusch, Martin Dichgans, Holger Lerche, Paola Gavazzo, Nikolaus Plesnila, and Tobias Freilinger. Hyperexcitable interneurons trigger cortical spreading depression in an *Scn1a* migraine model. *The Journal of Clinical Investigation*, 131(21), November 2021.
- [3] Ernest Barreto and John R. Cressman. Ion concentration dynamics as a mechanism for neuronal bursting. *Journal of Biological Physics*, 37(3):361–373, June 2011.
- [4] R.J. Butera Jr, J.W. Clark Jr, and J.H. Byrne. Transient responses of a modeled bursting neuron: Analysis with equilibrium and averaged nullclines. *Biological Cybernetics*, 77(5):307–322, November 1997.
- [5] Alexandru Călin, Andrei S. Ilie, and Colin J. Akerman. Disrupting Epileptiform Activity by Preventing Parvalbumin Interneuron Depolarization Block. *Journal of Neuroscience*, 41(45):9452–9465, November 2021.
- [6] Mario Cammarota, Gabriele Losi, Angela Chiavegato, Micaela Zonta, and Giorgio Carmignoto. Fast spiking interneuron control of seizure propagation in a cortical slice model of focal epilepsy. *The Journal of Physiology*, 591(4):807–822, 2013.
- [7] Sandrine Cestèle, Emanuele Schiavon, Raffaella Rusconi, Silvana Franceschetti, and Massimo Mantegazza. Non-functional NaV1.1 familial hemiplegic migraine mutant transformed into gain of function by partial rescue of folding defects. *Proceedings of the National Academy of Sciences*, 110(43):17546–17551, October 2013.
- [8] Yanqiu Che, Shuzhou Zhang, Jiang Wang, Shigang Cui, Chunxiao Han, Bin Deng, and Xile Wei. Synchronization of inhibitory coupled Hindmarsh-Rose neurons via adaptive sliding mode control. In *2nd International Conference on Intelligent Control and Information Processing*, volume 2, pages 1134–1139, 2011.
- [9] Oana Chever, Sarah Zerimech, Paolo Scalmani, Louisiane Lemaire, Lara Pizzamiglio, Alexandre Loucif, Marion Ayrault, Martin Krupa, Mathieu Desroches, Fabrice Duprat, Isabelle Léna, Sandrine Cestèle, and Massimo Mantegazza. Initiation of migraine-related cortical spreading depolarization by hyperactivity of GABAergic neurons and Nav1.1 channels. *The Journal of Clinical Investigation*, 131(21), November 2021.
- [10] Lieve Claes, Jurgen Del-Favero, Bertien Ceulemans, Lieven Lagae, Christine Van Broeckhoven, and Peter De Jonghe. De Novo Mutations in the Sodium-Channel Gene SCN1A Cause Severe Myoclonic Epilepsy of Infancy. *The American Journal of Human Genetics*, 68(6):1327–1332, June 2001.

- [11] John R. Cressman, Ghanim Ullah, Jokubas Ziburkus, Steven J. Schiff, and Ernest Barreto. The influence of sodium and potassium dynamics on excitability, seizures, and the stability of persistent states: I. Single neuron dynamics. *Journal of Computational Neuroscience*, 26(2):159–170, April 2009.
- [12] Mathieu Desroches, John Guckenheimer, Bernd Krauskopf, Christian Kuehn, Hinke M. Osinga, and Martin Wechselberger. Mixed-Mode Oscillations with Multiple Time Scales. *SIAM Review*, 54(2):211–288, January 2012.
- [13] Mathieu Desroches and Vivien Kirk. Spike-Adding in a Canonical Three-Time-Scale Model: Superslow Explosion and Folded-Saddle Canards. *SIAM Journal on Applied Dynamical Systems*, 17(3):1989–2017, January 2018.
- [14] Mathieu Desroches, Martin Krupa, and Serafim Rodrigues. Spike-adding in parabolic bursters: The role of folded-saddle canards. *Physica D: Nonlinear Phenomena*, 331:58–70, September 2016.
- [15] Sandra Dhifallah, Eric Lancaster, Shana Merrill, Nathalie Leroudier, Massimo Mantegazza, and Sandrine Cestèle. Gain of Function for the SCN1A/hNav1.1-L1670W Mutation Responsible for Familial Hemiplegic Migraine. *Frontiers in Molecular Neuroscience*, 11, 2018.
- [16] Martin Dichgans, Tobias Freilinger, Gertrud Eckstein, Elena Babini, Bettina Lorenz-Depiereux, Saskia Biskup, Michel D Ferrari, Jürgen Herzog, Arn MJM van den Maagdenberg, Michael Pusch, and Tim M Strom. Mutation in the neuronal voltage-gated sodium channel SCN1A in familial hemiplegic migraine. *The Lancet*, 366(9483):371–377, July 2005.
- [17] Eusebius J. Doedel, Alan R. Champneys, Fabio Dercole, Thomas F. Fairgrieve, Yuri A. Kuznetsov, Bart E. Oldeman, Randy C. Paffenroth, Björn Sandstede, Xianjun J. Wang, and Chenghai H. Zhang. AUTO-07P: Continuation and bifurcation software for ordinary differential equations. 2007.
- [18] G. B. Ermentrout and N. Kopell. Parabolic Bursting in an Excitable System Coupled with a Slow Oscillation. *SIAM Journal on Applied Mathematics*, 46(2):233–253, April 1986.
- [19] Michel D. Ferrari, Roselin R. Klever, Gisela M. Terwindt, Cenk Ayata, and Arn M. J. M. van den Maagdenberg. Migraine pathophysiology: Lessons from mouse models and human genetics. *The Lancet Neurology*, 14(1):65–80, January 2015.
- [20] Richard FitzHugh. Impulses and Physiological States in Theoretical Models of Nerve Membrane. *Biophysical Journal*, 1(6):445–466, July 1961.
- [21] Gerson Florence, Tiago Pereira, and Jürgen Kurths. Extracellular potassium dynamics in the hyperexcitable state of the neuronal ictal activity. *Communications in Nonlinear Science and Numerical Simulation*, 17(12):4700–4706, December 2012.
- [22] John Guckenheimer and Yuri A. Kuznetsov. Hopf-Hopf bifurcation. *Scholarpedia*, 3(8):1856, August 2008.
- [23] J. L. Hindmarsh and R. M. Rose. A model of the nerve impulse using two first-order differential equations. *Nature*, 296(5853):162–164, March 1982.
- [24] Niklas Hübel and Markus A. Dahlem. Dynamics from Seconds to Hours in Hodgkin-Huxley Model with Time-Dependent Ion Concentrations and Buffer Reservoirs. *PLOS Computational Biology*, 10(12):e1003941, December 2014.
- [25] Nico A. Jansen, Anisa Dehghani, Margot M. L. Linssen, Cor Breukel, Else A. Tolner, and Arn M. J. M. van den Maagdenberg. First FHM3 mouse model shows spontaneous cortical spreading depolarizations. *Annals of Clinical and Translational Neurology*, 7(1):132–138, 2020.
- [26] Keisuke Kaneko, Christopher B. Currin, Kevin M. Goff, Eric R. Wengert, Ala Somarowthu, Tim P. Vogels, and Ethan M. Goldberg. Developmentally regulated impairment of parvalbumin interneuron synaptic transmission in an experimental model of Dravet syndrome. *Cell Reports*, 38(13):110580, March 2022.
- [27] Christopher M. Kim and Duane Q. Nykamp. The influence of depolarization block on seizure-like activity in networks of excitatory and inhibitory neurons. *Journal of Computational Neuroscience*, 43(1):65–79, August 2017.
- [28] Marc T. M. Koper. Bifurcations of mixed-mode oscillations in a three-variable autonomous Van der Pol-Duffing model with a cross-shaped phase diagram. *Physica D: Nonlinear Phenomena*, 80(1):72–94, January 1995.
- [29] Louisiane Lemaire, Mathieu Desroches, Martin Krupa, Lara Pizzamiglio, Paolo Scalmani, and Massimo Mantegazza. Modeling NaV1.1/SCN1A sodium channel mutations in a microcircuit with realistic ion concentration dynamics suggests differential GABAergic mechanisms leading to hyperexcitability in epilepsy and hemiplegic migraine. *PLOS Computational Biology*, 17(7):e1009239, July 2021.
- [30] Camille Liautard, Paolo Scalmani, Giovanni Carriero, Marco de Curtis, Silvana Franceschetti, and Massimo Mantegazza. Hippocampal hyperexcitability and specific epileptiform activity in a mouse model of Dravet syndrome. *Epilepsia*, 54(7):1251–1261, 2013.

- [31] Sebastian Major, Shufan Huo, Coline L. Lemale, Eberhard Siebert, Denny Milakara, Johannes Woitzik, Karen Gertz, and Jens P. Dreier. Direct electrophysiological evidence that spreading depolarization-induced spreading depression is the pathophysiological correlate of the migraine aura and a review of the spreading depolarization continuum of acute neuronal mass injury. *GeroScience*, 42(1):57–80, February 2020.
- [32] Massimo Mantegazza and Vania Broccoli. SCN1A/NaV1.1 channelopathies: Mechanisms in expression systems, animal models, and human iPSC models. *Epilepsia*, 60(S3):S25–S38, 2019.
- [33] Massimo Mantegazza and Sandrine Cestèle. Pathophysiological mechanisms of migraine and epilepsy: Similarities and differences. *Neuroscience Letters*, 667:92–102, February 2018.
- [34] Massimo Mantegazza, Sandrine Cestèle, and William A. Catterall. Sodium channelopathies of skeletal muscle and brain. *Physiological Reviews*, 101(4):1633–1689, October 2021.
- [35] J. Nagumo, S. Arimoto, and S. Yoshizawa. An Active Pulse Transmission Line Simulating Nerve Axon. *Proceedings of the IRE*, 50(10):2061–2070, October 1962.
- [36] John C. Oakley, Franck Kalume, Frank H. Yu, Todd Scheuer, and William A. Catterall. Temperature- and age-dependent seizures in a mouse model of severe myoclonic epilepsy in infancy. *Proceedings of the National Academy of Sciences*, 106(10):3994–3999, March 2009.
- [37] Daniela Pietrobon and Michael A. Moskowitz. Chaos and commotion in the wake of cortical spreading depression and spreading depolarizations. *Nature Reviews Neuroscience*, 15(6):379–393, June 2014.
- [38] John Rinzel. Bursting oscillations in an excitable membrane model. In *Ordinary and Partial Differential Equations*, Lecture Notes in Mathematics, pages 304–316. Springer, Berlin, Heidelberg, 1985.
- [39] John Rinzel. A formal classification of bursting mechanisms in excitable systems. In *Mathematical Topics in Population Biology, Morphogenesis and Neurosciences*, pages 267–281. Springer, Berlin, Heidelberg, 1987.
- [40] Ana Rita Salgueiro-Pereira, Fabrice Duprat, Paula A. Pousinha, Alexandre Loucif, Vincent Douchamps, Cristina Regondi, Marion Ayrault, Martine Eugie, Marion I. Stunault, Andrew Escayg, Romain Goutagny, Vadym Gnatkovsky, Carolina Frassoni, Hélène Marie, Ingrid Bethus, and Massimo Mantegazza. A two-hit story: Seizures and genetic mutation interaction sets phenotype severity in SCN1A epilepsies. *Neurobiology of Disease*, 125:31–44, May 2019.
- [41] Krasimira Tsaneva-Atanasova, Hinke M. Osinga, Thorsten Rieß, and Arthur Sherman. Full system bifurcation analysis of endocrine bursting models. *Journal of Theoretical Biology*, 264(4):1133–1146, June 2010.
- [42] Shigeki Tsuji, Tetsushi Ueta, Hiroshi Kawakami, Hiroshi Fujii, and Kazuyuki Aihara. Bifurcations in two-dimensional hindmarsh-rose type model. *International Journal of Bifurcation and Chaos*, 17(03):985–998, March 2007.
- [43] Ghanim Ullah, Yina Wei, Markus A. Dahlem, Martin Wechselberger, and Steven J. Schiff. The Role of Cell Volume in the Dynamics of Seizure, Spreading Depression, and Anoxic Depolarization. *PLOS Computational Biology*, 11(8):e1004414, August 2015.
- [44] Yangyang Wang and Jonathan E. Rubin. Timescales and Mechanisms of Sigh-Like Bursting and Spiking in Models of Rhythmic Respiratory Neurons. *The Journal of Mathematical Neuroscience*, 7(1):3, June 2017.
- [45] Yina Wei, Ghanim Ullah, and Steven J. Schiff. Unification of Neuronal Spikes, Seizures, and Spreading Depression. *Journal of Neuroscience*, 34(35):11733–11743, August 2014.
- [46] Frank H. Yu, Massimo Mantegazza, Ruth E. Westenbroek, Carol A. Robbins, Franck Kalume, Kimberly A. Burton, William J. Spain, G. Stanley McKnight, Todd Scheuer, and William A. Catterall. Reduced sodium current in GABAergic interneurons in a mouse model of severe myoclonic epilepsy in infancy. *Nature Neuroscience*, 9(9):1142–1149, September 2006.
- [47] Jokubas Ziburkus, John R. Cressman, Ernest Barreto, and Steven J. Schiff. Interneuron and Pyramidal Cell Interplay During In Vitro Seizure-Like Events. *Journal of Neurophysiology*, 95(6):3948–3954, June 2006.